Title

Aspergillus fumigatus Hsp90 interacts with the main components of the cell wall integrity pathway and cooperates in heat shock and cell wall stress adaptation.

Journal

Cellular Microbiology, 23(2)

Authors

Rocha, Marina

Minari, Karine

Fabri, João

et al.

Publication Date

2021-02-01

DOI

10.1111/cmi.13273

Peer reviewed

HHS Public Access

Author manuscript

Cell Microbiol. Author manuscript; available in PMC 2022 February 01.

Published in final edited form as:

Cell Microbiol. 2021 February ; 23(2): e13273. doi:10.1111/cmi.13273.

Aspergillus fumigatus Hsp90 interacts with the main components of the cell wall integrity pathway and cooperates in heat shock and cell wall stress adaptation

Marina Campos Rocha[1], **Karine Minari**[1,2], **João Henrique Tadini Marilhano Fabri**[1], **Joshua D. Kerkaert**[3], **Lisandra Marques Gava**[1], **Anderson Ferreira da Cunha**[1], **Robert A. Cramer**[3], **Júlio César Borges**[2], **Iran Malavazi**[1]

[1]Departamento de Genética e Evolução, Centro de Ciências Biológicas e da Saúde, Universidade Federal de São Carlos, São Carlos, SP, Brazil.

[2]Instituto de Química de São Carlos, Universidade de São Paulo, São Carlos, SP, Brazil.

[3]Department of Microbiology and Immunology, Geisel School of Medicine at Dartmouth, Hanover, NH, USA.

Abstract

The initiation of *Aspergillus fumigatus* infection occurs via dormant conidia deposition into the airways. Therefore, conidial germination and subsequent hyphal extension and growth occur in a sustained heat shock (HS) environment promoted by the host. The Cell Wall Integrity Pathway (CWIP) and the essential eukaryotic chaperone Hsp90 are critical for fungi to survive HS. Although *A. fumigatus* is a thermophilic fungus, the mechanisms underpinning the HS response are not thoroughly described and important to define its role in pathogenesis, virulence, and antifungal drug responses. Here, we investigate the contribution of the CWIP in *A. fumigatus* thermotolerance. We observed that the CWIP components PkcA, MpkA, and RlmA are Hsp90 clients and that a PkcA^{G579R} mutation abolishes this interaction. PkcA^{G579R} also abolishes MpkA activation in the short-term response to HS. Biochemical and biophysical analyses indicated that Hsp90 is a dimeric functional ATPase, which has a higher affinity for ADP than ATP and prevents MpkA aggregation *in vitro*. Our data suggest that the CWIP is constitutively required for *A. fumigatus* to cope with the temperature increase found in the mammalian lung environment, emphasizing the importance of this pathway in supporting thermotolerance and cell wall integrity.

*Corresponding author: imalavazi@ufscar.br.

Author contributions

I.M, J.C.B., L.M.G., M.C.R. and K.M., designed, interpreted and validated the experiments involving protein expression and analyses. I.M., M.C.R., J.H.T.M.F, and A.F.C. designed, interpreted and validated gene and protein expression analyses. I.M., R.A.C and J.D.K. designed fluorescent microscopy experiments, analyzed and interpreted the data. M.C.R, K.M., J.H.T.M.F., J.D.K. and I.M performed experiments. I.M. conceived the study and wrote the manuscript. All authors discussed the data, edited and approved the manuscript.

Competing interests

The authors declare no competing interests.

Data Availability Statement

The data that supports the findings of this study are available in the supplementary material of this article

Keywords

Cell wall integrity; Heat shock; Hsp90; PkcA; MpkA; *Aspergillus fumigatus*

Introduction

Aspergillus fumigatus is the most common *Aspergillus* species to cause systemic infections in humans (Latge & Chamilos, 2019). The clinical spectrum of aspergillosis varies, but preexisting immunosuppression is most often associated with establishment of invasive pulmonary aspergillosis, the most severe form of infection that accounts for high mortality rates (van de Veerdonk *et al.*, 2017, Brown *et al.*, 2012, Brown *et al.*, 2014, Sugui *et al.*, 2014, Kousha *et al.*, 2011). *A. fumigatus* is a thermophilic saprophytic fungus that can grow at temperatures up to 55 °C and survive as conidia at temperatures up to 70 °C (Araujo & Rodrigues, 2004, Albrecht *et al.*, Brakhage & Langfelder, 2002, Rhodes & Askew, 2010). Therefore, this attribute of *A. fumigatus* biology allows adaptation to temperatures found before and after infection mammalian hosts. In contrast, other species such as *A. flavus, A. terreus* and *A. niger* are less tolerant to germination and growth at higher temperatures (Weber *et al.*, 2009, Perfect *et al.*, 2001, Araujo & Rodrigues, 2004). Such species are also less commonly as causing invasive infection (Hedayati *et al.*, 2007).

The initiation of *A. fumigatus* infection occurs via dormant conidia deposition into the airways. Therefore, conidial germination and subsequent hyphal extension and growth occur in a sustained heat shock (HS) environment found in mammalian hosts. It has long been hypothesized that thermotolerance significantly contributes to *A. fumigatus* pathogenicity (Albrecht *et al.*, 2010, Rhodes, 2006, Bhabhra & Askew, 2005). While many studies have focused on defining differentially expressed genes during HS, few molecules have been thoroughly investigated to comprehensively link the function of these proteins to heat adaptation and virulence (Albrecht *et al.*, 2010, Bhabhra & Askew, 2005, Do *et al.* 2009, Chang *et al.*, 2004, Zhou *et al.*, 2007, Sueiro-Olivares *et al.*, 2015).

Elevated temperature causes protein damage and misfolding leading to altered and potential loss of protein function. Hsp90 (90 kDa heat shock protein) is a conserved and essential eukaryotic molecular chaperone that mediates proteostasis (McClellan *et al.*, 2007, Zhao *et al.*, 2005, Schopf *et al.*, 2017). The ATP-dependent Hsp90 machine assists a subset of proteins involved in several cellular processes during posttranslational folding and macromolecular assembly. Numerous Hsp90 client proteins are protein kinases, transcription factors (TF) and other signaling proteins involved in key signal transduction pathways (Taipale *et al.*, 2012). Pivotal studies in fungi have shown that when Hsp90 function is compromised, the rapid evolution of resistance to azoles and echinocandins in fungal pathogens such as *Candida albicans* and *A. fumigatus* is abrogated (Cowen & Lindquist, 2005, Cowen *et al.*, 2009, Singh *et al.*, 2009, Lamoth *et al.*, 2014a).

In addition to altered protein function, heat stress impacts the essential fungal cell wall (CW). One signaling cascade widely employed by fungi to maintain cell viability in response to different sources of stresses including thermal stress is the Cell Wall Integrity Pathway (CWIP) (Altwasser *et al.*, 2015, Bruder Nascimento *et al.*, 2016, Rocha *et al.*, 2015,

Valiante *et al.*, 2009). The apical kinase of the CWIP, PkcA, is central to the signaling through this cascade and leads to the activation of the downstream MAP kinase MpkA and the activation of the TF RlmA (Rocha *et al.*, 2020, Rocha *et al.*, 2016, Rocha *et al.*, 2015). CWIP-mediated transcriptional responses allow cells to prioritize the remodeling and repair of CW damage; thus, linking drug susceptibility and morphogenesis (LaFayette *et al.*, 2010, Altwasser *et al.*, 2015).

Cooperating mechanisms between the CWIP and Hsp90 function have been observed in *A. fumigatus* since mutants of these genes are concomitantly more susceptible to CW stress and elevated temperatures (Lamoth *et al.*, 2012, Rocha *et al.*, 2015, Valiante *et al.*, 2009). Also, *hsp90* mediates the caspofungin paradoxical effect (Aruanno *et al.*, 2019, Lamoth *et al.*, 2014a, Lamoth *et al.*, 2014b). At the protein level, the MpkA homologs in yeast and *C. albicans* are known Hsp90 clients (LaFayette *et al.*, 2010, Diezmann *et al.*, 2012). However, the molecular mechanisms underpinning Hsp90's function in *A. fumigatus* CW integrity remains unknown.

Here, we investigated the contribution of the *A. fumigatus* CWIP proteins PkcA, MpkA and RlmA in thermotolerance and their functional and physical interactions with Hsp90. We observe that PkcA and Hsp90 physically interact in *A. fumigatus*, and the PkcA^{G579R} mutation abolishes this interaction. Biochemical and biophysical analyses indicate that Hsp90 is a dimeric functional ATPase, which prevents MpkA aggregation *in vitro*.

Results

Cell wall integrity pathway (CWIP) mutants are less tolerant to heat shock (HS)

Previous results indicated that *A. fumigatus* CWIP mutants colony radial growth on solid media is impacted at 45 °C (Rocha *et al.*, 2016). To further assess the link between CW integrity and thermotolerance, we quantified the susceptibility of the CWIP mutants to HS. The viability of conidia exposed to HS for 12 and 24 h at 45 °C or 50 °C was significantly reduced in comparison to the wild-type strain. Viability of conidia was about 75% lower in both *pkcA*^{G579R} and Δ*mpkA* strains exposed to 45 °C, and this value was strikingly as low as 83% and 95% for the same strains incubated at 50 °C for 12 h. The reduction in the viability of Δ*rlmA* conidia reached 35% and 65% after 12 h of incubation at 45 °C and 50 °C, respectively (Fig. 1A). These results suggest that high temperature HS can be fungicidal to conidia from these mutant strains. Subsequently, we investigated the metabolic activity of the mature *A. fumigatus* biofilm consisting of hyphal cells exposed to HS. The 2,3-bis-(2-methoxy-4-nitro-5-sulfophenyl)-2H-tetrazolium-5-carboxanilide salt (XTT) assay was employed to test the biofilm response to HS as previously described (Dhingra *et al.*, 2018). Consistent with the observed decrease in conidia viability, biofilms of *pkcA*^{G579R} and Δ*mpkA* strains also exhibited a significant decrease in metabolic activity when the biofilm was incubated for 60 or 120 min at 48 °C (Fig. 1B). This reduction in metabolic activity reached about 50% for the *pkcA*^{G579R} mutant and was more severe for the Δ*mpkA* strain (60% and 78%, respectively). In contrast, no significant reduction in metabolic activity was observed for the Δ*rlmA* strain. The biofilms obtained for the *pkcA*^{G579R} and Δ*mpkA* strains were very fragile, and the use of collagen-coated plates was crucial to maintain and stabilize the biofilm during the experiment. The surface of the *pkcA*^{G579R} and Δ*mpkA* mutants has

reduced extracellular matrix and altered composition of the carbohydrates exposed at the cell wall, as reported previously (Manfiolli *et al.*, 2018, Rocha *et al.*, 2015). Metabolic activity of the biofilms at the baseline was similar since four times higher amount of Δ*mpkA* conidia was inoculated to achieve similar growth rate and equal glucose consumption, as described earlier (Jain *et al.*, 2011). These results reinforce the observation that thermotolerance is significantly impaired when key protein kinases of the CWIP are deficient. The lack of a phenotype for the Δ*rlmA* strain during biofilm HS suggests other un-studied transcriptional regulators downstream of the canonical CWIP protein kinase are involved at the time points studied.

PkcA-dependent MpkA phosphorylation is required for early adaptation to HS

A critical consequence of HS is the transcriptional activation of chaperones and co-chaperones that are part of the cell responses to withstand the temperature increase. To probe further into the contribution of the CWIP to HS, we used biofilm hyphae to measure the mRNA levels of selected genes predicted to encode chaperone and co-chaperone proteins and known CWIP protein encoding genes. This list of genes includes the chaperones *hsp90* (AFUB_052690) (Lamoth *et al.*, 2012) and the two cytosolic *hsp70,* i. e., *hsp70* (AFUB_007770); and *hscA* (AFUB_083640; *Saccharomyces cerevisiae SSB*1/*SSB2* homologs) previously characterized (Lamoth *et al.*, 2015). In addition, we included the non-characterized genes: *hsp30*-like protein (AFUB_072390); which encodes a putative integral plasma membrane heat shock protein (Dinamarco *et al.*, 2012), *ssc70* (AFUB_025800; yeast *SSC1*), which possibly encodes a mitochondrial Hsp70, similar to the human mortalin, and the *A. fumigatus* homolog of the HS transcriptional regulator *hsf1* (AFUB_050430; *S. cerevisiae* and *C. albicans HSF1* homolog). Most of these genes encode proteins known to be Hsp90 clients or required for the Hsp90 cycle and ATP hydrolysis (O'Meara *et al.*, 2019). We observed that mRNA abundance of *pkcA*, *mpkA* and *rlmA* was induced at least 2 $\log_2$ -fold in the wild-type strain after 30 min of HS at both 37 °C and 48 °C, respectively, further supporting their expected role in the HS response in *A. fumigatus* (Fig. 2A–B and Fig. S1). Importantly, the mRNA levels of *pkcA* increased the most among all the tested CWIP genes, reaching about 3.8 $\log_2$ -fold increase post 120 min HS at 37 °C (Fig. S1). Interestingly, there was an increase in the mRNA levels of *pkcA* (4 to 4.8 $\log_2$-fold) in the Δ*mpkA* mutant at 48 °C and a significant decrease in the mRNA levels of *rlmA* in the *pkcA*^{G579R} and Δ*mpkA* strains at both temperatures. As expected, there were significant increases in the mRNA abundance of genes involved in HS response in the wild-type strain, such as the chaperone *hsp90*, which was 3.6 $\log_2$ -fold induced after 30 min of HS at both temperatures. The only exception was the *hscA* chaperone. We observed marked decreases in the mRNA levels of *hsfA*, *hsp90* and *hsp70* genes at both temperatures in the three CWIP mutants. Altogether, these data indicate that the mRNA levels of predicted *A. fumigatus* HS effectors are in part controlled by key regulators of the *A. fumigatus* CWIP.

The transcriptional analysis indicated that *pkcA* is very important for HS adaptation including the host's physiological temperature (37 °C). Based on this observation, we constructed PkcA::GFP fusions for both the wild-type and the G579R variant under the control of the native promoter to investigate the subcellular localization of PkcA during HS. Under standard laboratory conditions, confocal microscopy revealed that both PkcA:: GFP

and PkcA^{G579R}::GFP localizes at the hyphal tips (dome shape), septum and sites of branching (Fig. 2C), as previously described for *A. nidulans* (Teepe *et al.*, 2007). To quantitatively determine if PkcA::GFP and PkcA^{G579R}::GFP showed differences in localization at the population level prior to and during HS, the percent number of hyphal tips containing tip localized PkcA was determined for both isoforms of PkcA over time (Fig. 2D, upper table panel). To further quantify localization dynamics at the individual hyphae level, a tip enrichment score was calculated (Fig. 2D) by taking the tip fluorescence and dividing by the fluorescence of the adjacent cytoplasm for each hyphal tip, as demonstrated in Fig. S2 and Data File 1. This quantification revealed that under non-HS conditions (0 min), wild-type PkcA had a significantly higher degree of enrichment at the hyphal tip in comparison to the PkcA^{G579R} isoform ($p<0.0001$). From a biological standpoint the tip enrichment score is indicative of the degree to which cells bias the localization of PkcA, and differences may be suggestive of a difference in initial response potential to stress. On the application of HS treatment, both isoforms of PkcA moved from the previously observed sites of accumulation and became distributed throughout the cytosol, without any differences between the isoforms observed in the first 8-minutes post HS (Fig. 2C–D). At 10- and 12-minutes post-HS the PkcA^{G579R} isoform began returning to the hyphal tips, with 52.4% and 67.2% tip localization, respectively. In contrast, the percent tip localization for the wild-type PkcA at 10- and 12-minutes post-HS remained low at 24.5% and 20.6%, respectively (Fig. 2D, upper panel $p<0.05$ and $p<0.001$, respectively). Consistently, the wild-type PkcA's tip enrichment score was significantly lower than PkcA^{G579R} at these timepoints (Fig. 2D). Together these results indicate the G579R mutation results in faster recruitment of PkcA back to the hyphal tip after HS. Additionally, signs of cell lysis were observed exclusively in the *pkcA*^{G579R}::GFP strain shortly after application of HS (Fig. S2C), along with a small population of germlings (less than 5% of the population) showing an accumulation of PkcA^{G579R} in vesicle-like structures (Fig. S2D). Our data suggests that wild-type PkcA spends more time in the cytosol after HS, and this brief sub cellular relocation likely orchestrates the HS response before it is recruited again to the hyphal tips. Although PkcA^{G579R} isoform regains baseline tip localization sooner, the susceptibility of the mutant strain to elevated temperatures suggests that this dynamic is associated with the deficient HS response.

To further understand the contribution of CWIP regulators to thermotolerance and HS, we investigated the activation of this pathway by assessing the phosphorylation status of the MAP kinase MpkA after HS up to 240 min. The MpkA phosphorylation at 37 °C was maintained at constant levels in both the wild-type and Δ*rlmA* mutant during HS (Fig. S3). In the *pkcA*^{G579R} mutant strain there was a small but highly reproducible increase in MpkA phosphorylation in the replicate experiments after 30 to 240 min of HS. In contrast to the results at 37 °C, when the cells were exposed to 48 °C, MpkA was rapidly phosphorylated in the wild-type strain (10–15 min) and followed by a large drop in phosphorylation after the initial increase (Fig. 2E). MpkA phosphorylation in the Δ*rlmA* strain at 48 °C was similar to wild-type, though a single phosphorylation peak was detected after 10 min of HS. In contrast to the results at 37 °C, phosphorylated MpkA was absent in the *pkcA*^{G579R} strain at all time points tested at 48 °C. These data suggest that PkcA is critical to phosphorylate MpkA in response to severe HS.

Taken together, these results suggest that PkcA is the critical upstream protein kinase of the CWIP in response to HS conditions, and that MpkA is an important downstream effector phosphorylated through a PkcA dependent mechanism to activate and sustain the HS response, including key chaperones such as Hsp90.

Hsp90 inhibition causes loss of viability of the CWIP mutants

The observation that *hsp90* mRNA levels are reduced in the CWIP regulator mutants (Fig. 2) prompted us to investigate whether Hsp90 would be required for the CWIP response by assessing the susceptibility of the CWIP mutant strains to the Hsp90 inhibitors radicicol and geldanamycin (Fig. 3A–B). All the CWIP mutant strains showed higher sensitivity to these compounds in comparison to the wild-type strain. The viability was determined via alamar blue reduction and the IC_{50} for each strain was calculated based on an inhibitor versus normalized response model. This analysis showed that all the CWIP mutants are significantly more susceptible to radicicol and geldanamycin than the wild-type strain (Fig. 3C–D and Table S1).

Subsequently, we investigated Hsp90 protein levels in the *pkcA*^{G579R}, Δ*rlmA* and Δ*mpkA* mutants during HS. At 37 °C, Hsp90 protein levels did not significantly change in the wild-type and in the Δ*rlmA* mutant strain. Consistent and small increases in Hsp90 abundance occurred up to 120 min of HS for *pkcA*^{G579R} and Δ*mpkA* strains (Fig. S4). However, when cells were incubated at 48 °C, the Hsp90 abundance rapidly increased in the wild-type strain early after 10 min. The rapid increase in Hsp90 protein levels was delayed for all CWIP mutants as noticeable increased expression was observed only after 30–120 min of HS (Fig. 3). Taken together, these results indicate that Hsp90 is important for the CWIP in response to HS in part through a PkcA mediated mechanism.

PkcA, MpkA and RlmA are constitutive Hsp90 clients in *A. fumigatus*

Consequently, we next questioned whether Hsp90 physically interacts with the *A. fumigatus* CWIP components. As a first approach to address this question, we utilized Co-immunoprecipitation (Co-IP) experiments for each component of the CWIP when cells were exposed to HS (at 37 °C or 48 °C) or CW stress induced by congo red (CR). Consistent with our results suggesting Hsp90 and PkcA working together to mediate the CWIP response to HS, our Co-IP experiments identified a non-described protein-protein interaction in fungi between Hsp90 and PkcA under these conditions (Fig. 4). We next further dissected the significance of the conserved cysteine-rich domain (C1B) of PkcA in this interaction (Fig. 4A), through introduction of a G579R mutation into the *pkcA::*3×HA tagged strain and analyzed the Hsp90 interaction with this mutated isoform. The *pkcA*^{G579R} is a hypomorphic mutation initially identified in *A. nidulans pkcA* isolated in a genetic screen that identified hypersensitivity strains to calcofluor white (Teepe *et al.*, 2007). The *pkcA*^{G579R} allele is located at a conserved site immediately beside the C1B regulatory domain (Fig. 4A). We observed that the point mutation G579R abolished this interaction at both conditions tested (Fig. 4C). These results suggest that the C1B domain of PkcA may be required for the physical interaction of Hsp90 and PkcA in *A. fumigatus* and that the conformational changes likely caused by this G to R substitution impair Hsp90-PkcA recognition.

To further validate this novel observation, we expressed a C-terminally truncated form of both the wild-type and G579R mutated PkcA in *E. coli*, which encompasses the residues 409–1106 and harbors most of the regulatory domains of PkcA (Fig. 4A). Despite many efforts, PkcA(409–1106) was expressed only in the insoluble form, which precluded the use of the protein in functional pull-down assays. Therefore, given this experimental limitation, we decided to use this *E. coli* expression system to perform Far Western blot (FWB) analysis. In brief, FWB can detect specific protein-protein interaction in a complex mixture of proteins and is particularly useful for examining interactions between proteins that are difficult to analyze by other methods due to solubility problems or because they are difficult to express in cells (Edmondson & Roth, 2001, Jadwin *et al.*, 2015, Wu *et al.*, 2007). Accordingly, *E. coli* extracts containing PkcA(409–1106) or PkcA(409–1106)^{G579R} proteins were immobilized on PVDF membrane and then probed with purified and folded Hsp90, which was subsequently detected by α-Hsp90. In support of the *in vivo* data, FWB recapitulated the results of the Co-IP and confirmed the lack of Hsp90 interaction with the mutated protein (Fig. S5A–B). Our FWB analysis also suggest that the two HR1 and C2 domains are not essential for Hsp90 interaction with PkcA.

We importantly also detected an MpkA interaction with Hsp90 in our Co-IP experiments with previous reports in *C. albicans* (LaFayette *et al.*, 2010) (Fig. 4D). Consequently, as an additional control for the FWB experiments with Hsp90 and PkcA, we ran a parallel FWB where MpkA was immobilized onto PVDF membrane, probed with purified and folded Hsp90 and detected by the antibody (Fig. S5C). As expected, the results confirmed the Hsp90 and MpkA interaction observed by Co-IP and further support the observed FWB results with PkcA.

Interestingly, we also detected an interaction between Hsp90 and RlmA in *A. fumigatus*, which has not been described in either *S. cerevisiae* or *C. albicans* to date (Fig. 4E). These results are consistent with our previous report which indicated that *rlmA* and *mpkA* genetically interact to maintain cell homeostasis during CW and heat stresses (Rocha *et al.*, 2016). In line with this idea, we observed that MpkA and RlmA physically associate constitutively (Fig. S6A). Based on this finding, we assumed that Hsp90 interaction with RlmA could be indirect since these three proteins may exist as a complex inside the nucleus when the CWIP is activated. We next tested whether RlmA and Hsp90 directly interact and used the yeast two-hybrid assay (Y2H) as an additional test to ascertain this interaction (Fig. S6B–C). The results indicate that bait-RlmA interacted with prey-Hsp90 (and vice versa) and supports the results observed by Co-IP. Altogether, these data indicate that Hsp90 physically interacts with the main described regulators of the CWIP in *A. fumigatus*. Given that all the interactions observed in Fig. 4 were also detected in the control condition, we conclude that CWIP proteins constitutively interact with Hsp90 in *A. fumigatus*.

Recombinant *A. fumigatus* Hsp90 binds ADP and ATP with different affinities and is a functional ATPase

To gain a deeper understanding of *A. fumigatus* Hsp90 function and to evaluate its main structural properties, we successfully cloned and expressed rAfHsp90 in *E. coli* as described

in the materials and methods section and Table S2. The efficiency of the protein purification was assessed by 10% SDS-PAGE yielding highly purified Hsp90 (Fig. 5A).

As a first approach to assess structural properties of the rAfHsp90, circular dichroism (CD) spectropolarimetry and intrinsic tryptophan fluorescence spectroscopy were used to analyze secondary and local tertiary structures of the protein, respectively. The CD spectra presented a similar profile to that reported for different Hsp90 orthologues, with secondary structure content estimated as 33% of α-helix, 17% of β-sheets, 17% of turns and 33% of random coils (Fig. 5B), also similar to previous characterizations (Minari *et al.*, 2019, Silva *et al.*, 2013). The intrinsic emission fluorescence spectra for Hsp90 (Fig. 5C) indicated a maximum emission wavelength (λ_{max}) at around 334 nm, suggesting that the five Trp residues in the polypeptide are buried or partially protected from the solvent. In the presence of the denaturing agent guanidine hydrochloride (Gnd-HCl), the spectra underwent a red shift, and the λ_{max} changed to 351 nm, indicating the protein denaturation and Trp exposition to the solvent. Altogether, these data indicate rAfHsp90 was obtained properly folded.

Analytical size-exclusion chromatography (aSEC) was used to assess protein hydrodynamic properties such as the Stokes radii (Rs) and protein shape. The elution profile of the rAfHsp90 in comparison to that of the standard protein mix indicated that it presents an estimated apparent molecular mass (MM_{app}) of 430 ± 30 kDa, suggesting that it could be arranged as a pentamer in solution (Fig. 5D–E). The estimated Rs for rAfHsp90 was 68 ± 2 Å leading to a frictional ratio of 1.85 ± 0.06, which can be due to the elongated shape attributed to Hsp90 as dimers. Similar results were reported for Hsp90 of *Leishmania braziliensis* (Silva *et al.*, 2013), which is a highly elongated and flexible dimer in solution (Seraphim *et al.*, 2017) and is 63% identical to AfHsp90. Likewise, our results suggest that rAfHsp90 is probably a highly elongated dimer in solution.

It is known that the low ATPase activity of Hsp90 is required for the chaperone cycle and this enzymatic activity relies on the N-domain dimerization as well as the synergistic interaction with different co-chaperones and resulting conformational changes (Schopf *et al.*, 2017). Based on these features, the ATP hydrolysis rate varies in different species (Minari *et al.*, 2019, Chatterjee & Tatu, 2017). To evaluate the functionality of the rAfHsp90, we determined its binding affinities to ADP and ATP by isothermal titration calorimetry (ITC), which also allowed obtaining the thermodynamic parameters of the nucleotide binding. We observed that the interactions between rAfHsp90 and the natural ligands were exothermic as represented by the negative peaks of the isothermograms (Fig. 6A–B). The interaction with ATP showed an apparent enthalpy change (ΔH_{app}) of −4600 ± 800 cal mol^{-1} and an apparent entropy change (ΔS_{app} of +5 ± 1 cal mol^{-1} K^{-1}, suggesting a process driven by both enthalpy and entropy (Fig. 6A). It is also observed that interaction with ADP has a higher ΔH_{app} (−11500 ± 700 cal mol^{-1}), indicating that the reaction is enthalpically driven but showed an entropic penalty (ΔS_{app}) of −16 ± 2 cal mol^{-1} K^{-1} (Fig. 6B). The estimated interaction stoichiometry indicated that 2 adenosine nucleotide interacts with 1 Hsp90 dimer in solution. Fig. 6C depicts the thermodynamic signature for rAfHsp90 interaction with adenosine nucleotides. As observed for Hsp90 orthologues (Minari *et al.*, 2019), the rAfHsp90 interaction with adenosine nucleotides present different thermodynamic

signatures. Interactions with ATP are driven by both enthalpy and entropy, while interactions with ADP are highly driven by enthalpy and have an entropic penalty. These results indicate molecular interaction differences with such molecules. In spite of that, the apparent Gibbs energy change (ΔG_{app}) was around −6.3 to −6.8 kcal mol^{-1} which means binding affinities in the same order reflecting in dissociation constants (K_D) of 12 ± 2 μM to ADP and 24 ± 2 μM to ATP. These values are in the same range of those determined to Hsp90 orthologues in the same conditions (Minari *et al.*, 2019). To mention some orthologues previously studied, AfHsp90 is 61%, 64% and 75% identical to Hsp90 of *Plasmodium falciparum*, human (alpha isoform) and yeast, respectively (Minari *et al.*, 2019). rAfHsp90 showed low ATPase activity as evaluated by the kinetic parameters obtained by the Michaelis-Menten fitting of the ATPase activity rate (Fig. 6D). The data indicated a Michaelis constant (K_M) of 231 μM and a turnover number (k_{cat}) of 0.47 min^{-1}. These values are of the same order as that reported for Hsp90 orthologues and consistent with a cycling mechanism involving multiple conformational changes. Altogether, these results indicated that rAfHsp90 obtained here has all signatures of a folded and functional Hsp90.

Biochemical properties of recombinant MpkA

We initially explored the biochemical properties of MpkA since this is the first report of a successful filamentous fungal MAP kinase recombinant expression. The expression conditions are described in Table S2, and the efficiency of the protein purification assessed by 10% SDS-PAGE is shown in Fig. S7A. The results indicated that highly purified recombinant MpkA (rAfMpkA) was obtained. Again, CD spectropolarimetry and intrinsic tryptophan fluorescence spectroscopy were used to analyze secondary and local tertiary structures of this protein. The CD spectra presented a similar profile to that reported for different rAfMpkA orthologues, such as the human ERK2 and the *Arabidopisis thaliana* MAP kinase (51% and 50.6% identity with MpkA, respectively) for which resolved crystallographic structures are available (PDB ID: 1PME and 5CI6, respectively) (Fox *et al.*, 1998, Wang *et al.*, 2016). Our results indicated that rAfMpkA presents secondary structure content estimated as 34% of α-helix, 16% of β-sheets, 17% of turns, and 32% of random coils (Fig S7B). The intrinsic emission fluorescence spectra for rAfMpkA (Fig. S7C) indicated a λ_{max} at around 336 nm, suggesting that the four Trp residues in the polypeptide are buried or partially protected from the solvent. In the presence of the denaturing agent guanidine hydrochloride (Gnd-HCl), the spectra underwent a red shift, and the λ_{max} changed to 347 nm, indicating the protein denaturation and Trp exposition to the solvent.

The elution profile of the MpkA in comparison to that of the standard protein mix obtained by aSEC indicated that rAfMpkA presents an Rs of 31 ± 1 Å and an MM_{app} estimated as 55 ± 4 kDa, suggesting that it is arranged as a globular monomer in solution (Fig. S7D–E), since the calculated frictional ratio was 1.24 ± 0.04. Similar results were reported for the His-tagged human ERK2, which was massively present as a monomer in solution, as observed by SEC coupled with multi-angle laser light scattering and analytical ultracentrifugation (Callaway *et al.*, 2006, Kaoud *et al.*, 2011). Human ERK proteins are monomers in the non-phosphorylated state, although they can form dimers *in vitro*, which are necessary for MAP kinase activity (Khokhlatchev *et al.*, 1998, Philipova & Whitaker, 2005, Casar *et al.*, 2008). Nevertheless, monomeric ERK2 was reported to specifically

associate with nuclear proteins (Casar *et al.*, 2008). Altogether, our results strongly suggest that rAfMpkA is a monomer in solution that presents all the signatures of a folded and functional MAP kinase. Additional investigation is needed to understand the *in vivo* structural modifications of MpkA and their relevance in the context of the CWIP signaling.

Hsp90 has chaperone activity and prevents aggregation of MpkA

Here, we demonstrated by Co-IP and FWB that MpkA interacts with Hsp90, even in the non-HS condition (Fig. 4 and Fig. S5), suggesting that MpkA may constitutively require the chaperone activity of Hsp90 and undergo thermal instability during HS. With the observed functionality of the rAfHsp90, we sought to investigate if direct chaperone activity could be recorded between rAfHsp90 and rAfMpkA, as it has been described that Hsp90 can stabilize proteins, such as citrate synthase and malate dehydrogenase (MDH) and protect them from aggregation in a temperature-induced aggregation model (Silva *et al.*, 2013).

Initially, we verified the aggregation properties of rAfMpkA by incubating increasing concentrations of folded MpkA at 42 °C up to 120 min. Although MpkA did not lose its secondary structure when subjected to high temperatures, as observed by the CD signal upon heating (data not shown), and was stable up to 50 min of incubation at 42 °C, it had a high aggregation profile after incubation at 42 °C for 120 minutes(Fig. 7A). Our tests revealed that rAfHsp90 protected rAfMpkA from aggregation in a dose-dependent manner even in a substoichiometric concentration (1 rAfHsp90:2 rAfMpkA) leading to 25% prevention of MpkA aggregation (Fig. 7B). The maximum prevention values were 76% when rAfHsp90 was added in a 5-fold molar excess (5 rAfHsp90:1 rAfMpkA). As an additional control, we performed a similar experiment to measure the ability of rAfHsp90 to prevent the aggregation of a known Hsp90 client: the human MDH (Fig. 7C). The values were similar (about 76%) using the same molar ratio (5 rAfHsp90:1 MDH). Taken together, these results reinforce that MpkA is an Hsp90 client and that this chaperone is fully functional *in vitro*.

Discussion

A. fumigatus experiences HS when initiating infection and the initial cell divisions after breaking the dormancy of the conidia occur under constant HS conditions imposed by the human host. There is limited information in *A. fumigatus* connecting thermotolerance and the cellular regulators of fungal stress adaptation, including the CWIP and Hsp90. Previous reports have shown that inhibition of Hsp90 causes increased susceptibility to antifungals. The increased susceptibility to caspofungin in Hsp90 depleted cells is of particular interest because it links the function of Hsp90 and the CWIP (LaFayette *et al.*, 2010, Lamoth *et al.*, 2012, Lamoth *et al.*, 2014b). Here, we revealed that the main components of the CWIP interreact with the Hsp90, including the TF RlmA, described as an Hsp90 client for the first time in any fungus (Fig. 8). We provide evidence that PkcA is crucial for the short-term response to HS in a MpkA-dependent manner and that the C1B domain of the PkcA is important for Hsp90 interaction. We propose that identifying the specific interplay between Hsp90 and the CWIP can add new information on how to navigate towards a specific Hsp90 inhibitor as a tool to weaken the fungal CW and disrupt thermotolerance.

We reciprocally confirmed the relationship between Hsp90 and the CWIP mutants by observing that *pkcA*^{G579R}, Δ*mpkA* and Δ*rlmA* were highly susceptible to HS and pharmacological inhibition of Hsp90 (Figs. 1 and 3). Also, HS response requires early activation of CWIP, as observed by the increased MpkA phosphorylation upon HS, which is mostly dysregulated in the Δ*rlmA* or absent in the *pkcA*^{G579R} strains (Fig. 2). The lack of MpkA phosphorylation in the *pkcA*^{G579R} mutant is unexpected while potentially reflects the absence of the upcoming signal to the three-component MAP kinase cascade activation. We previously showed during CW stress, there is a decrease in the MpkA phosphorylation if PkcA activity is genetically or pharmacologically perturbed (Rocha *et al.*, 2015). Here, our data suggest that HS response via CWIP is highly dependent on a fully functional PkcA. Previous reports also suggest that HS and CR sensitivity is sensed via the mechanosensor MidA (Fig. 8) that signals though PkcA-MpkA circuitry (Dichtl *et al.*, 2012, Samantaray *et al.*, 2013) and not surprisingly, thermosensitivity of Δ*mpkA* strain is more severe than the sensitivity caused by sublethal concentration of CW stressing agents (Valiante *et al.*, 2009). Interestingly, MpkA was quickly phosphorylated in wild-type after 10 min of HS, indicating that this event is essential for short term heat adaptation. This nonetheless differs to what was observed in *C. albicans*, in which Mkc1^{MpkA} is linked to long term adaptation to HS (Leach *et al.*, 2012a). We provide evidence that CWIP in *A. fumigatus* is required at the beginning of thermal adaptation, concomitantly with the presumably function of HsfA-Hsp90 regulatory circuit (Leach *et al.*, 2012c, Leach *et al.*, 2012b, Nicholls *et al.*, 2009), which is central to short-term initiation of HS response in eukaryotes, but not investigated here. Consistently, the increase in MpkA phosphorylation exactly coincides with the increase in Hsp90 abundance after 10 min of HS, which is severely delayed in the CWIP mutants, but robustly sustained up to 120 min after HS in all mutant strains (Fig 3). So, we suggest that the CWIP is a crucial element in heat adaptation in *A. fumigatus,* with a much earlier role in comparison to *C. albicans*. This feature can ultimately point to the differences in the mold lifestyle and may support the intrinsic thermophilic nature of *A. fumigatus*.

We showed that three components of the *A. fumigatus* CWIP are Hsp90 clients (Figs. 4 and S5–6). On the one hand, this finding is not surprising for the MAPK MpkA, since their orthologues are known Hsp90 clients (Zhao *et al.*, 2005, LaFayette *et al.*, 2010). On the other hand, we demonstrated that the CWIP apical kinase PkcA and the downstream TF RlmA are part of the growing list of the fungal Hsp90 clientele. One of the most interesting and unexpected findings of this study is that *rlmA* is playing a minor role in supporting thermotolerance downstream of *mpkA*, despite its importance in the maintenance of the CW integrity (Rocha *et al.*, 2016), thus suggesting that other unidentified TFs regulate adaptation to temperature fluctuations in *A. fumigatus*. Quantitative analyses of Hsp90 clients in human cells indicated that only 7% of the clients are TFs. In humans, MEF2B (myocyte-specific enhancer factor) associates with the essential co-chaperone Cdc37, which binds to *HSP90* early in the chaperone cycle (Taipale *et al.*, 2012). MEF2B is the closest RlmA homolog (50% identity, 6e-21), and our results suggest that in fungi, the interaction of this TF with the Hsp90 machinery is direct, without co-chaperone intervention (Fig. S6).

These two non-reported Hsp90 physical interactions reflect the plasticity of this chaperone, whose interaction network varies widely according to environmental cues (Diezmann *et al.*, 2012, Lamoth *et al.*, 2016, O'Meara *et al.*, 2019). Similar to what is reported in mammalian

cancer cells, in which Hsp90 assists the stabilization of tumorigenic cells by buffering oncogenic mutations and protecting oncoproteins that are considered “addicted” to Hsp90 (Li *et al.*, 2012), we argue that a similar landscape occurs in fungi in that the CWIP is a primary target of Hsp90. Supporting this notion, we demonstrate that the Hsp90 stabilizes the CWIP components even under control conditions, suggesting that they are constitutively chaperoned (buffered) by Hsp90 (Fig. 4). In fact, we demonstrated Hsp90 chaperone activity on MpkA *in vitro* (Fig. 7), where no other potential partners or facilitatory events occur, thus reinforcing the biological significance of the constitutive *in vivo* interaction observed by the Co-IP experiments. Our data suggest that this interaction occurs with Hsp90 in both open and closed states since neither co-chaperones nor adenosine nucleotides were added in the reaction cell. Notably, we did not detect interaction between Hsp90 and the MAP kinase of the HOG (High Osmolarity Glycerol) pathway SakA by Co-IP under CW stressing conditions (data not shown), again suggesting the prominent role of the CWIP in thermotolerance.

Here, we identified a potential region of the PkcA protein which is important for Hsp90 interaction since the G579R mutation abolished the Hsp90-PkcA recognition. With the exception of some Hsp90 interactors for which a defined structural determinant is known (Schopf *et al.*, 2017), we still have only a rudimentary understanding of what determines client protein binding by Hsp90. There is no typical interaction domain between Hsp90 and its clientele, which encompass a wide range of proteins with unrelated amino acid sequences and functions. It has been suggested that protein surface electrostatics features and active conformation, rather than the primary sequence, define the capacity of the Hsp90 to recognize client kinases (Taipale *et al.*, 2010, Schopf *et al.*, 2017, Citri *et al.*, 2006, Luo *et al.*, 2017). The PkcA^{G579R} mutation is located juxtaposed outside the formal boundaries of the C1B domain (Figs. 4A and 8), which is present in conventional, novel and fungal PKC isoforms and a known binding site for the second messenger diacylglycerol (DAG) in conventional and novel, but not in fungal PKCs (Newton, 2018, Schmitz & Heinisch, 2003, Herrmann *et al.*, 2006, Teepe *et al.*, 2007). In mammalian cells, Hsp90 is reported to interact with conventional PKCβII via a conserved Pro residue in the PxxP motif of the C-terminal tail of the kinase, which we also identified in PkcA (Fig. 4A). Mutations in these two Pro result in a kinase that is not activated by priming phosphorylation which does not bind Hsp90 and Cdc37 (Gould *et al.*, 2009). In the absence of the resolved structure of fungal PKC’s, confident PkcA modeling to understand the impact of the G579R substitution is not feasible. Thus, it remains to be determined if a perturbation on the tertiary structure of PkcA impairs the Hsp90-PkcA^{G579R} interaction or whether C1B vicinity is a fungal-specific Hsp90 interaction domain. For the same reasons, it is difficult to conclude why both the wild-type and the mutated PkcA isoform reside in the hyphal tip (Fig. 2) or what is the exact meaning of the reallocation of this protein to the cytosol during HS. It is known that the C1 domain of Pkc1 binds to the small GTPase Rho1 in *S. cerevisiae* (Nonaka *et al.*, 1995). Based on the yeast model [reviewed in Heinisch and Rodicio (2018) and references therein], Pkc1 resides at the cytosol in an inactive form. Activation is primed by phosphorylation by upstream kinases (not yet identified in *A. fumigatus*). Since C1B domain of fungal PKCs do not respond to DAG, Rho1 protein could be the recruiting component of the inactive protein to the membrane via HR1 domains (Fig. 8) by binding other lipids, such as

phosphatidylserine (Nomura *et al.*, 2017, Ryckbosch *et al.*, 2017). C1 domains then associate to the plasma membrane's inner leaf, relieve the hindrance caused by the pseudosubstrate over the catalytic site domain, which folds properly to allow accommodation of ATP substrate within the C-terminal tail (Schmitz *et al.*, 2001, Schmitz & Heinisch, 2003). Active Pkc1 then phosphorylates its target proteins, which can be downstream CWIP targets (Fig. 8). In a laser damage wound-healing model, yeast Pkc1 disappears from the resident budding sites and subsequently appears at the cell wall/membrane at the laser-induced damage site after 8.8 min to promote cell recovery (Kono *et al.*, 2012). It is tempting to speculate that the disappearance of PkcA during HS in *A. fumigatus* occurs with the same dynamics as the observed in laser wounded yeast in an Hsp90-independent manner and the return to the hyphal tip is a physiological consequence since these are the areas of de novo growth, which are more sensitive to temperature fluctuations and cell wall damaging agents. As shown in Fig. 2, the initial response potential may be altered given that the tip-to-cytoplasmic protein ratio is lower in the mutant at baseline, and that the duration of the response/signaling may not be sufficient to confer resistance to stress since we observe $PkcA^{G579R}$ isoform returning to the hyphal tips sooner. We can also suggest that the recruitment of unchaperoned $PkcA^{G579R}$ isoform is accompanied by an inefficient repositioning of the mutated C1B domain in the inner membrane leaf that is not ideal for promoting or sustaining the activation of PkcA (Fig. 8).

In conclusion, our results have contributed significantly towards the understanding of how CWIP actively participates in the regulation of thermotolerance in *A. fumigatus* and add information about the importance of Hsp90 in the events coordinated by this signaling cascade. Moreover, we report the first demonstration of the main biochemical properties of Hsp90 and MpkA in fungi and the identification of a single residue substitution that abolishes Hsp90 interaction with PkcA. Further structural characterization of the CWIP proteins will be an essential step to define how these interactions take place to mediate their critical role in fungal pathogenesis and antifungal drug responses.

Materials and Methods

Strains and culture conditions

The *A. fumigatus* strains used in this study are described in Table S3. All the strains were maintained in complete (YG) or minimal medium (MM), as described previously (Malavazi & Goldman, 2012). To grow *pyrG*$^{-}$ auxotrophic strains, the media was supplemented with 1.2 g/L of uridine and uracil. If required, pyrithiamine (Sigma) or hygromycin (Millipore) was added to the culture medium in a concentration of 0.1 μg/mL or 200 μg/mL, respectively. Liquid cultures to produce biofilm hyphae of the relevant strains exposed to HS were obtained by inoculating 1×10^7 conidia in 50 mL of MM for 24 h at 30 °C and subsequently heat-shocked at 37 °C or 48 °C with pre-warmed fresh MM for 15, 30 or 60 min. To induce CW stress, the cultures were grown in MM at 37 °C and subjected to CR exposure for 30 min with the required concentrations indicated in each experiment. For the Δ*mpkA* strain, the amount of conidia used was four times that of the wild-type strain to achieve equal glucose consumption (Jain *et al.*, 2011). Mycelia from each time point were

collected via vacuum filtration, flash-frozen in liquid nitrogen and stored at −80°C until used for either protein or RNA extractions.

Susceptibility of the CWIP mutants to thermal stress

The susceptibility of conidia to high temperature was accessed accordingly to (Richie *et al.*, 2009). Briefly, 1×10^2 conidia of each strain were inoculated in solid MM and incubated at 45 °C or 50 °C for 12 and 24 h. Subsequently, plates were incubated at 37 °C for 24 h. The percentage of survival was obtained by CFU counting in comparison to the control plates (30 °C). The 2,3-bis-(2-methoxy-4- nitro-5-sulfophenyl)-2H-tetrazolium-5-carboxanilide salt (XTT) assay was used to measure the metabolic activity of mature *A. fumigatus* biofilm, as previously reported (Moss *et al.*, 2008). Briefly, 1×10^5 conidia were incubated in 500 μL of MM in 24-well plates and biofilm was formed by 22 h of incubation at 37 °C, followed by an incubation at 30 °C for 2 h. Due to the defect in the $pkcA^{G579R}$ and Δ*mpkA* strains to form biofilm, plates were coated with collagen (Cell Applications) prior to inoculation in order to facilitate cell adhesion and stabilization of the biofilm. Control plates were maintained at this temperature, while thermal stress was induced in the biofilm by incubating the plates at 45 °C for 1 or 2 h. Absorbances measured at 490 nm from the treated and control plates were used to calculate the percentage of reduction in the metabolic activity based on the XTT reduction that generates a water-soluble formazan product.

Susceptibility assays to Hsp90 inhibitors

To evaluate the susceptibility of the CWIP mutants in the presence of Hsp90 inhibitors, 1×10^3 conidia of each strain were grown in 0.2 mL of liquid MM in 96-well plates supplemented with varying concentrations of the drugs. To monitor growth, 10% alamar blue (Thermo Fisher) was used as previously reported (Rocha et al., 2018). The plates were incubated for 48 h at 37 °C and photographed. To generate the survival curves, 100 μL of culture medium was placed in black 96-well plates (CellStar 650086) and the fluorescence intensities (λ=590 nm) of treated and untreated samples (n=4) for each strain were obtained after 24 and 48 hours of incubation (37 °C), according to the manufacturer's protocol. The values were used to calculate the percentage of viability. Data were fit with a nonlinear regression following a variable slope model of [inhibitor] vs. normalized response in GraphPad Prism version 8.4.3 according to the following equation. $Y = 100/(1 + (IC50/X)\text{^}HillSlope)$. No special handling of outlier was enabled, and no curve fitting restraints were included. From this model, the inhibitory concentration 50 (IC50) and its 95% confidence interval were calculated for each strain using the likelihood ratio asymmetric method.

RNA extraction, cDNA preparation and RT-qPCR procedures

Mycelia obtained under HS at 37 °C and 48 °C were disrupted by grinding in liquid nitrogen with a pestle and mortar. The total RNA was extracted with Trizol reagent (Thermo Scientific) according to the manufacturer's protocol. The samples were treated with Turbo DNase I (Ambion Thermo Scientific) according to the manufacturer's protocol and processed as described previously for cDNA synthesis (Rocha *et al.*, 2015). The primers for the individual genes were designed using Primer Express 3.0 software (Thermo Scientific) and are listed in Table S4. Three independent biological replicates were used, and the

relative $\log_2$ fold change in mRNA quantity was calculated using the comparative cycle threshold (Ct) (ΔΔCt) analysis (Livak & Schmittgen, 2001). All values were normalized to the expression of the *A. fumigatus* β-tubulin (*tubA*) gene. The $\log_2$ fold change values were submitted to a hierarchical clustering algorithm (Euclidian distance) by using the TMEV software (available at http://www.tm4.org/mev.html). Statistical analysis was performed using one-way ANOVA with Tukey's *posttest* to assess differences in the mutant strains compared to the same growth condition in the wild-type strain ($p \leq 0.05$).

Generation of GFP- and 3×HA-tagged strains

PkcA and PkcA^{G579R} containing C-terminal fusions with GFP protein or 3×HA epitope were constructed using the Δ*akuB* and pkcA^{G579R} *pyrG*$^{-}$ as recipient strains. The *pkcA*^{G579R} *pyrG*$^{-}$ strain was obtained by the spontaneous loss of the *pyrG* prototrophy marker upon 5-FOA treatment. The strategies and primers used to generate the substitution cassettes are described in Fig. S8 and Table S5, respectively. The GFP::*pyrG* fragment was amplified from the plasmid pRS426-*prxC* (Rocha *et al.*, 2018) using the primers Spacer GFP pyrG and pyrG REV, while the 3×HA::*pyrG* fragment was amplified from the plasmid pOB430 using the primers linker 3×HA-pyrG FW pOB430 and linker 3×HA-pyrG REV pOB430. The gene replacement cassettes were constructed by *in vivo* recombination in *S. cerevisiae* following the description in (Malavazi & Goldman, 2012). In brief, they consisted of a 1 kb 3' fragment of *pkcA* gene (without the stop codon) that was cloned in-frame with the GFP or 3×HA fragments. Transformants were validated by PCR with primers pkcA start SC and pkcA 3R 3×HA or pkcA start SC and pyrG 200 REV to confirm each tagged strain. The sensitivities of these strains to growth under 30 °C, 37 °C and 48 °C high temperature or in the presence of CR were comparable to the wild-type strain, indicating that these alleles are fully functional (Fig. S8I).

Fluorescent microscopy

pkcA::GFP or *pkcA*^{G579R}::GFP tagged strains were cultured on glass-bottom dishes (Matek) in 2 mL of MM at 37 °C for 10 h and for 1 additional hour at room temperature. Subsequently, the medium was removed and 2 mL of fresh pre-warmed media (48 °C) was added to induce HS in the germlings. Images were acquired every 2 minutes up to 12 min after HS with a 63× oil-immersion objective (Nikon) using 488 nm laser line and an Andor W1 Spinning Disk Confocal with a Nikon Eclipse Ti inverted microscope stand. Due to toxicity when HS was combined with the laser, a different field of view was used for every timepoint. Images were processed and quantified using imageJ Fiji (Schindelin *et al.*, 2012, Rueden *et al.*, 2017). Sum Z-projections were generated, and the background subtracted using the rolling ball method set to 50 pixels. To quantify tip localization a tip enrichment score was generated by quantifying the sum fluorescence within a 3 μm diameter circle at the hyphal tip and dividing that by the sum fluorescence of the adjacent cytoplasm within a 3 μm diameter circle (Fig S2A–B). Hyphal tips with a tip enrichment score ≥ 1.3 were considered tip localized. At least 96 germlings were quantified for every timepoint in the wild-type strain across 4 biological replicates, and at least 189 germlings were quantified for every timepoint in the *pkcA*^{G579R}*::GFP* strain across 6 biological replicates. To determine differences in the degree of tip enrichment between the two strains, a two-way ANOVA with Sidak's multiple comparisons test was used.

Protein extraction, immunoblotting analysis and Hsp90 antibody production

For protein extractions used for Western blots, 0.5 mL of lysis buffer was added to the ground mycelia as described previously (Rocha *et al.*, 2015). For Western blots, 50 μg of protein from each sample were resolved in 12% SDS-PAGE and transferred to PVDF membranes (GE Health Care). Detection of MpkA was achieved by using α-(phospho) P-p44/42 and α-p44/42 MAPK antibodies (Cell Signaling Technologies; 9101 and 9107) according to previous descriptions (Bruder Nascimento *et al.*, 2016, Rocha *et al.*, 2015). α-γ-tubulin (Santa Cruz Biotechnology; yN-20;) was used as the loading control as previously reported (Rocha *et al.*, 2018). Western blot signals were quantitated using ImageJ and normalized to total MpkA protein levels. For the detection of the 3×FLAG and 3×HA epitopes, mouse monoclonal α-FLAG or α-HA antibodies were used (Sigma; F1804 and H3663, respectively) as previously reported (Rocha *et al.*, 2020). The *A. fumigatus* Hsp90 was detected using a custom polyclonal α-Hsp90 antibody raised in rabbit and produced by Imuny, Rheabiotech, Brazil (IM-0199, Batch 16057). Full-length recombinant Hsp90 tagged with 6×His expressed in *E. coli* and purified as described in the procedures below were used in the immunizations. Raised antibody was purified by G protein affinity chromatography. α-Hsp90 was used at a 1:20,000 dilution in TBST solution containing 5% skimmed milk for 16 h at 4 °C. The secondary antibody incubations were performed at room temperature for 2 h using α-rabbit IgG-HRP (Sigma; A0545) and 1:5,000 dilution. For all experiments, chemoluminescent detection was achieved by using an ECL Prime Western Blot detection kit (GE HealthCare). Images were generated by exposing the PVDF membranes to the ChemiDoc XRS gel imaging system (BioRad). The images were subjected to densitometric analysis using the ImageJ software (Schneider *et al.*, 2012) and normalized to total MpkA or γ-tubulin protein levels (Figs. 2 and 3, respectively).

Co-immunoprecipitation (Co-IP) procedures

Strains carrying 3×HA or 3×FLAG epitopes were submitted to either HS at 37 °C or 48 °C for 15 min or CW stress induced by CR exposure (10, 100 and 300 μg/mL) during 30 min. To Co-IP 3×HA-tagged strains, Dynabeads Protein A (Thermo Fisher Scientific) coated with α-HA antibody (Sigma; H3663) were used as described in (Fabri *et al.*, 2018). For the Co-IP of RlmA::3×FLAG, the same conditions were employed but using 20 μL of α-Flag M2 Affinity Gel (Sigma; A2220). Cell extracts and agarose resin were then incubated with shaking at 4 °C for 2 h. To release the proteins from the resins, samples were incubated with 30 μL of 2× Laemmli buffer and boiled for 5 min. 20 μL of the immunoprecipitated samples were run in a 10% SDS-PAGE. Proteins were electroblotted for Western blot assay.

Two-hybrid yeast assay

The coding sequences of *rlmA* and *hsp90* were cloned in-frame into pGBKT7 (bait) or pGADT7 (prey) vectors, respectively, according to the manufacture's recommendation for the Matchmaker Gold Yeast Two-Hybrid System (Clonetch). The plasmid pGBKT7-rlmA was transformed into Y2H-Gold strain cells while the empty pGADT7 or the construct pGADT7-hsp90 was transformed into the Y187 strain cells. The transformed yeasts were mated for 24 h at 30 °C and plated on synthetic double dropout selection medium (DDO), which lacks Trp and Leu for selection of mated strains. Positive interaction between bait and

prey was assessed in high stringency quadruple dropout selection medium (QDO), which is deficient in Leu, Trp, His, adenine and supplemented with X-α-Gal (40 μg/mL) and 200 ng/mL of aureobasidin A (QDO/X/A). Plates were incubated at 30 °C for 5 days. Growth in the QDO/X/A media indicates bait and prey fusion proteins interaction, so the DNA-BD and AD are brought into proximity to activate transcription of four independent reporter genes (*AUR1, ADE2, HIS3,* and *MEL1*). Positive and negative interaction controls were applied to the same selection plates.

Cloning the *hsp90*, *mpkA*, *rlmA* and truncated *pkcA*(409–1106) genes

The sequences of the *hsp90* (AFUB_052690), *mpkA* (AFUB_070630) and *rlmA* (AFUB_040580) transcripts were obtained from FungiDB (https://fungidb.org/fungidb/) and used to design primers for reverse transcription reactions (Table S6) using the enzyme SuperScript III Reverse Transcriptase (Thermo Fisher Scientific) according to the manufacture's recommendation. Full-length cDNA of *hsp90* and *mpkA* were obtained from a HS-induced culture of CEA17 wild-type strain. A C-terminal truncated version of the *pkcA* (AFUB_059540) gene spanning the nucleotides 1224 to 3321 of the transcript, which comprised the residues 409–1106, was synthesized and cloned in pUC19 (Epoch Life Sciences, USA) due to the failure of cDNA amplification. All the PCR products were cloned in the pET15b (Millipore Sigma) expression vector using the Gibson Assembly system (New England Biolabs), according to the manufacture's protocol. To generate the clone pkcA(409–1106) carrying the G579R mutation, the abovementioned pET15b-pkcA(409–1106) was subjected to site-directed mutagenesis using the QuikChange II XL Site-Directed Mutagenesis Kit (Agilent Technologies). All the individual clones were validated by full sequencing.

Protein expression and purification

Single colonies of *E. coli* BL21 Rosetta harboring each individual plasmids: pET15b-pkcA(409–1106), pET15b-pkcA(409–1106)^{G579R}, pET15b-mpkA and pET15b-hsp90 were grown in LB (100 μg/mL ampicillin and 35 μg/mL chloramphenicol) for 16 h (37 °C). The culture was diluted to OD_{600} 0.1 in 1 L of LB and cultured at 37 °C until the OD_{600} reached 0.6. IPTG was then added following the expression conditions shown in Table S2. Cells were harvested by centrifugation, washed and resuspended in 25 mM sodium phosphate buffer (pH 7.5) containing 500 mM NaCl [Hsp90 and PkcA(409–1106) cells] or 10 mM Tris, 5 mM sodium phosphate, 100 mM NaCl, 1 mM EDTA buffer [MpkA cells]. The cell suspensions were incubated on ice for 40 min after the addition of 30 μg/mL of lysozyme (Sigma) and 5 U DNAse (Sigma). Cells were lysed by sonication, centrifuged at 43,000 *g*, and the supernatant filtered with a 0.45 μm membrane. Proteins were purified according to Silva *et al.* (2013) with modifications. Briefly, the purifications were performed in two steps: affinity chromatography using a HisTrap column (GE Healthcare), followed by size exclusion chromatography using a Superdex 200 26/60 column (GE Healthcare) prepared in 40 mM HEPES (pH 7.5) buffer containing 100 mM KCl. Both purifications were performed with columns coupled to an Äkta Prime Plus (GE Healthcare) and using the same buffer as the mobile phase. Protein purification was evaluated by 10% SDS-PAGE. Recombinant protein concentrations were determined spectrophotometrically at 280 nm. The extinction

coefficients for reduced proteins were determined using the ProtParam tool (http://www.expasy.ch/tools/protparam.html) and are shown in Table S2.

Hydrodynamic characterization of recombinant Hsp90 and MpkA proteins

Analytical size exclusion chromatography (aSEC) experiments were carried out and analyzed according to Silva *et al.* (2013).

Spectroscopy studies of Hsp90 and MpkA

Circular dichroism spectropolarimetry (CD) measurements for the evaluation of secondary structures were performed using the Jasco J-815 spectropolarimeter. The CD spectra were collected in a 0.2 mm path length quartz cell containing 2.5 μM of Hsp90 or 5 μM of MpkA in 40 mM HEPES (pH 7.5) buffer containing 100 mM KCl. The OriginPro 8.0 software was used for data analysis and processing through the equation:

$$[\theta] = \frac{\theta \times 100 \times MM}{C \times l \times n}$$

Where [θ] represents the average residual molar ellipticity, MM indicates protein molecular mass (Da), C is the protein concentration (in mg/mL), l is the cuvette optical path and n is the number of aminoacid residues. Spectra deconvolution and secondary structure estimation was done with the CDNN deconvolution (Bohm *et al.*, 1992).

The intrinsic fluorescence emission analysis was performed using a Varioskan LUX multimodal microplate reader (Thermo Fisher Scientific) to evaluate the local tertiary structure of Hsp90 and MpkA. One μM of each protein (monomer concentration in the same buffer abovementioned) was placed in a quartz cuvette. The excitation wavelength was 295 nm and the selected emission wavelengths ranged from 315 to 420 nm. To analyze chemical-induced unfolding, each protein was incubated for 1 hour at room temperature with 5 M of guanidine hydrochloride (Gnd-HCl).

Isothermal titration calorimetry (ITC) measurements of ATP/ADP binding to Hsp90

ITC experiments were used to measure the interaction of Hsp90 and its natural ligands ATP or ADP in the presence of Mg^{2+}. The assays were conducted as previously reported (Minari *et al.*, 2019) in a MicroCal ITC200 microcalorimeter (GE Healthcare).

Hsp90 ATPase activity

ATPase activity was determined according to the methods described previously using the EnzChek Phosphate Assay Kit (E-6646; Molecular Probes) to monitor the inorganic phosphate (Pi) released in solution (Silva *et al.*, 2013). Purified and folded AfHsp90 (2 μM; monomer concentration) was suspended in 40 mM HEPES (pH 7.5) buffer containing 100 mM KCl and 5 mM MgCl2, in the presence of ATP (0 to 3 mM) for 90 min at 37 °C. Subsequently, the samples containing the Pi hydrolyzed from ATP were incubated for 30 min (23 °C) with 0.2 U of purine nucleoside phosphorylase (PNP) and 0.2 μM of the chromogenic substrate 2-amino-6-mercapto-7-methyl-purine riboside (MESG). The absorbance (360 nm) was measured to quantify the Pi consumed in the reaction.

Quantification of released Pi was achieved by interpolation of a standard curve in the range of 0–60 μM of Pi. The negative control was represented by ATP alone. The amount of Pi released per minute (i.e. V_0 in μM/min) was plotted as a function of the ATP concentration (mM), and a Michaelis-Menten fitting was applied to obtain the kinetic parameters using the Origin software.

Far Western blot procedures

Cell lysates of *E. coli* expressing the relevant bait proteins were separated in a 10% SDS-PAGE and electroblotted to PVDF membrane following standard protocols. The proteins were subjected to *in locus* denaturation on the membrane according to the protocol described by Wu *et al.* (2007). Briefly, The PVDF membrane was soaked in fresh AC buffer (100 mM NaCl, 20 mM Tris (pH 7.6), 0.5 mM EDTA, 10% glycerol, 0.1% Tween-20, 2% skim milk and 1 mM DTT) containing different concentrations of Gnd-HCl (6, 3, 1 and 0.1 M) during 30 min for denaturing/renaturing the proteins bound to the membrane. Incubations with 6, 3 and 1 M of Gnd-HCl were done at room temperature while incubation with 0.1 M of Gnd-HCl was done at 4 °C. One last incubation in AC buffer lacking Gnd-HCL for complete renaturing was conducted at 4 °C for 1 hour. Membranes were blocked with 5% skim milk in the PBST buffer (4 mM KH_2PO_4, 16 mM Na_2HPO_4, 115 mM NaCl (pH 7.4) and 0.05%Tween-20) for 1 hour at room temperature. The membranes were probed with 15 μM of purified and folded Hsp90 (bait) in protein-binding buffer (100 mM NaCl, 20 mM Tris (pH 7.6), 0.5 mM EDTA, 10% glycerol, 0.1% Tween-20, 2% skim milk powder and 1 mM DTT) overnight at 4 °C. After bait incubation, membranes were washed three times with PBST for 10 min. Membranes were probed with the α-Hsp90 antibody and detected as described above. To detect PkcA or MpkA, rabbit α-His antibody (Sigma; H1029) was used at a 1:10,000 dilution in TBST solution containing 5% skim milk for 16 h at 4 °C. Secondary antibody α-rabbit IgG-HRP (1:10,000 dilution) was employed under de conditions described above.

In vitro chaperone activity of Hsp90

Chaperone activity assays were performed in 40 mM HEPES buffer (pH 7.5) containing 100 mM KCl with 0.25, 0.5, 0.75, 1, 2.5 and 5 μM of Hsp90 in the presence of 10 μM of MpkA protein, according to the previous description (Silva *et al.*, 2013). Briefly, the aggregation temperature is an indicator of protein stability and can be used to identify ligands that bind and confer structural stability to a protein of interest. The aggregation is evaluated by light scattering, which increases as protein undergoes aggregation under the tested conditions (Jakob *et al.*, 1995). The experiments were performed in a 96-well UV-Star Half-area (Greiner) plate at 42 °C and protein aggregation was monitored at 320 nm in a Varioskan LUX multimode microplate reader (Thermo Scientific) for 2 h. Controls containing rAf Hsp90 at the indicated concentrations were performed to verify the aggregation of this protein. As a negative control of chaperone activity, BSA was used at 1, 2.5, 5, 7.5, 10, 20, 30, 40 and 50 μM in the presence of 10 μM of MpkA. As the positive control, human malate dehydrogenase (MDH), a known Hsp90 client protein, was purchased from Sigma and used in the assay at the final concentration of 1 μM.

Supplementary Material

Refer to Web version on PubMed Central for supplementary material.

Acknowledgments

We thank FAPESP - Fundação de Amparo à Pesquisa do Estado de São Paulo; grant nos. 2015/17541-0; 2016/07870-9; 2017/19694-3 (I.M.) and 2014/07206-6; 2017/07335-9; 2017/26131-5 (J.C.B) and CNPq - Conselho Nacional de Desenvolvimento Científico e Tecnológico grant nos. 462383/2014-8 (I.M) and 471415/2013-8 (J.C.B) for funding. This work was supported by the efforts of R.A.C through funding by NIH National Institute of Allergy and Infectious Diseases (NIAID) (grant nos. R01AI130128 and R01AI146121). R.A.C holds an Investigators in Pathogenesis of Infectious Diseases Award from the Burroughs Wellcome Fund. J.D.K. is awarded with a training NIH/NIAID grant (T32AI007519). We are also indebted to Dr. Özgür Bayram and Dr. Gustavo H. Goldman for providing the pOB430 plasmid and Magda R. Ometto Patricio for technical support (FAPESP 2019/00967-5).

References

Albrecht D, Guthke R, Brakhage AA, and Kniemeyer O (2010) Integrative analysis of the heat shock response in Aspergillus fumigatus. BMC Genomics 11: 32. [PubMed: 20074381]

Altwasser R, Baldin C, Weber J, Guthke R, Kniemeyer O, Brakhage AA, Linde J, and Valiante V (2015) Network Modeling Reveals Cross Talk of MAP Kinases during Adaptation to Caspofungin Stress in Aspergillus fumigatus. PLoS One 10: e0136932. [PubMed: 26356475]

Araujo R, and Rodrigues AG (2004) Variability of germinative potential among pathogenic species of Aspergillus. J Clin Microbiol 42: 4335–4337. [PubMed: 15365039]

Aruanno M, Bachmann D, Sanglard D, and Lamoth F (2019) Link between Heat Shock Protein 90 and the Mitochondrial Respiratory Chain in the Caspofungin Stress Response of Aspergillus fumigatus. Antimicrobial agents and chemotherapy 63.

Bhabhra R, and Askew DS (2005) Thermotolerance and virulence of Aspergillus fumigatus: role of the fungal nucleolus. Med Mycol 43 Suppl 1: S87–93. [PubMed: 16110798]

Bohm G, Muhr R, and Jaenicke R (1992) Quantitative analysis of protein far UV circular dichroism spectra by neural networks. Protein Eng 5: 191–195. [PubMed: 1409538]

Brakhage AA, and Langfelder K (2002) Menacing mold: the molecular biology of Aspergillus fumigatus. Annu Rev Microbiol 56: 433–455. [PubMed: 12142473]

Brown GD, Denning DW, Gow NA, Levitz SM, Netea MG, and White TC (2012) Hidden killers: human fungal infections. Sci Transl Med 4: 165rv113.

Brown GD, Meintjes G, Kolls JK, Gray C, Horsnell W, Working Group from the, E.-A.R.M.W., Achan B, Alber G, Aloisi M, Armstrong-James D, Beale M, Bicanic T, Black J, Bohjanen P, Botes A, Boulware DR, Brown G, Bunjun R, Carr W, Casadevall A, Chang C, Chivero E, Corcoran C, Cross A, Dawood H, Day J, De Bernardis F, De Jager V, De Repentigny L, Denning D, Eschke M, Finkelman M, Govender N, Gow N, Graham L, Gryschek R, Hammond-Aryee K, Harrison T, Heard N, Hill M, Hoving JC, Janoff E, Jarvis J, Kayuni S, King K, Kolls J, Kullberg BJ, Lalloo DG, Letang E, Levitz S, Limper A, Longley N, Machiridza TR, Mahabeer Y, Martinsons N, Meiring S, Meya D, Miller R, Molloy S, Morris L, Mukaremera L, Musubire AK, Muzoora C, Nair A, Nakiwala Kimbowa J, Netea M, Nielsen K, O'Hern J, Okurut S, Parker A, Patterson T, Pennap G, Perfect J, Prinsloo C, Rhein J, Rolfes MA, Samuel C, Schutz C, Scriven J, Sebolai OM, Sojane K, Sriruttan C, Stead D, Steyn A, Thawer NK, Thienemann F, Von Hohenberg M, Vreulink JM, Wessels J, Wood K, and Yang YL (2014) AIDS-related mycoses: the way forward. Trends Microbiol 22: 107–109. [PubMed: 24581941]

Bruder Nascimento AC, Dos Reis TF, de Castro PA, Hori JI, Bom VL, de Assis LJ, Ramalho LN, Rocha MC, Malavazi I, Brown NA, Valiante V, Brakhage AA, Hagiwara D, and Goldman GH (2016) Mitogen activated protein kinases SakA(HOG1) and MpkC collaborate for Aspergillus fumigatus virulence. Molecular microbiology 100: 841–859. [PubMed: 26878695]

Callaway KA, Rainey MA, Riggs AF, Abramczyk O, and Dalby KN (2006) Properties and regulation of a transiently assembled ERK2.Ets-1 signaling complex. Biochemistry 45: 13719–13733. [PubMed: 17105191]

Casar B, Pinto A, and Crespo P (2008) Essential role of ERK dimers in the activation of cytoplasmic but not nuclear substrates by ERK-scaffold complexes. Mol Cell 31: 708–721. [PubMed: 18775330]

Chang YC, Tsai HF, Karos M, and Kwon-Chung KJ (2004) THTA, a thermotolerance gene of Aspergillus fumigatus. Fungal Genet Biol 41: 888–896. [PubMed: 15338574]

Chatterjee S, and Tatu U (2017) Heat shock protein 90 localizes to the surface and augments virulence factors of Cryptococcus neoformans. PLoS Negl Trop Dis 11: e0005836. [PubMed: 28783748]

Citri A, Harari D, Shohat G, Ramakrishnan P, Gan J, Lavi S, Eisenstein M, Kimchi A, Wallach D, Pietrokovski S, and Yarden Y (2006) Hsp90 recognizes a common surface on client kinases. J Biol Chem 281: 14361–14369. [PubMed: 16551624]

Cowen LE, and Lindquist S (2005) Hsp90 potentiates the rapid evolution of new traits: drug resistance in diverse fungi. Science 309: 2185–2189. [PubMed: 16195452]

Cowen LE, Singh SD, Kohler JR, Collins C, Zaas AK, Schell WA, Aziz H, Mylonakis E, Perfect JR, Whitesell L, and Lindquist S (2009) Harnessing Hsp90 function as a powerful, broadly effective therapeutic strategy for fungal infectious disease. Proceedings of the National Academy of Sciences of the United States of America 106: 2818–2823. [PubMed: 19196973]

Dhingra S, Buckey JC, and Cramer RA (2018) Hyperbaric Oxygen Reduces Aspergillus fumigatus Proliferation In Vitro and Influences In Vivo Disease Outcomes. Antimicrobial agents and chemotherapy 62.

Dichtl K, Helmschrott C, Dirr F, and Wagener J (2012) Deciphering cell wall integrity signalling in Aspergillus fumigatus: identification and functional characterization of cell wall stress sensors and relevant Rho GTPases. Molecular microbiology 83: 506–519. [PubMed: 22220813]

Diezmann S, Michaut M, Shapiro RS, Bader GD, and Cowen LE (2012) Mapping the Hsp90 genetic interaction network in Candida albicans reveals environmental contingency and rewired circuitry. PLoS genetics 8: e1002562. [PubMed: 22438817]

Dinamarco TM, Almeida RS, de Castro PA, Brown NA, dos Reis TF, Ramalho LN, Savoldi M, Goldman MH, and Goldman GH (2012) Molecular characterization of the putative transcription factor SebA involved in virulence in Aspergillus fumigatus. Eukaryotic cell 11: 518–531. [PubMed: 22345349]

Do JH, Yamaguchi R, and Miyano S (2009) Exploring temporal transcription regulation structure of Aspergillus fumigatus in heat shock by state space model. BMC Genomics 10: 306. [PubMed: 19586549]

Edmondson DG, and Roth SY (2001) Identification of protein interactions by far Western analysis. Curr Protoc Mol Biol Chapter 20: Unit 20 26.

Fabri J, Godoy NL, Rocha MC, Munshi M, Cocio TA, von Zeska Kress MR, Fill TP, da Cunha AF, Del Poeta M, and Malavazi I (2018) The AGC Kinase YpkA Regulates Sphingolipids Biosynthesis and Physically Interacts With SakA MAP Kinase in Aspergillus fumigatus. Front Microbiol 9: 3347. [PubMed: 30692984]

Fox T, Coll JT, Xie X, Ford PJ, Germann UA, Porter MD, Pazhanisamy S, Fleming MA, Galullo V, Su MS, and Wilson KP (1998) A single amino acid substitution makes ERK2 susceptible to pyridinyl imidazole inhibitors of p38 MAP kinase. Protein Sci 7: 2249–2255. [PubMed: 9827991]

Gould CM, Kannan N, Taylor SS, and Newton AC (2009) The chaperones Hsp90 and Cdc37 mediate the maturation and stabilization of protein kinase C through a conserved PXXP motif in the C-terminal tail. J Biol Chem 284: 4921–4935. [PubMed: 19091746]

Hedayati MT, Pasqualotto AC, Warn PA, Bowyer P, and Denning DW (2007) Aspergillus flavus: human pathogen, allergen and mycotoxin producer. Microbiology 153: 1677–1692. [PubMed: 17526826]

Heinisch JJ, and Rodicio R (2018) Protein kinase C in fungi-more than just cell wall integrity. FEMS Microbiol Rev 42.

Herrmann M, Sprote P, and Brakhage AA (2006) Protein kinase C (PkcA) of Aspergillus nidulans is involved in penicillin production. Applied and environmental microbiology 72: 2957–2970. [PubMed: 16598003]

Jadwin JA, Mayer BJ, and Machida K (2015) Detection and quantification of protein-protein interactions by far-western blotting. Methods in molecular biology 1312: 379–398. [PubMed: 26044019]

Jain R, Valiante V, Remme N, Docimo T, Heinekamp T, Hertweck C, Gershenzon J, Haas H, and Brakhage AA (2011) The MAP kinase MpkA controls cell wall integrity, oxidative stress response, gliotoxin production and iron adaptation in Aspergillus fumigatus. Molecular microbiology 82: 39–53. [PubMed: 21883519]

Jakob U, Lilie H, Meyer I, and Buchner J (1995) Transient interaction of Hsp90 with early unfolding intermediates of citrate synthase. Implications for heat shock in vivo. J Biol Chem 270: 7288–7294. [PubMed: 7706269]

Kaoud TS, Devkota AK, Harris R, Rana MS, Abramczyk O, Warthaka M, Lee S, Girvin ME, Riggs AF, and Dalby KN (2011) Activated ERK2 is a monomer in vitro with or without divalent cations and when complexed to the cytoplasmic scaffold PEA-15. Biochemistry 50: 4568–4578. [PubMed: 21506533]

Khokhlatchev AV, Canagarajah B, Wilsbacher J, Robinson M, Atkinson M, Goldsmith E, and Cobb MH (1998) Phosphorylation of the MAP kinase ERK2 promotes its homodimerization and nuclear translocation. Cell 93: 605–615. [PubMed: 9604935]

Kono K, Saeki Y, Yoshida S, Tanaka K, and Pellman D (2012) Proteasomal degradation resolves competition between cell polarization and cellular wound healing. Cell 150: 151–164. [PubMed: 22727045]

Kousha M, Tadi R, and Soubani AO (2011) Pulmonary aspergillosis: a clinical review. Eur Respir Rev 20: 156–174. [PubMed: 21881144]

LaFayette SL, Collins C, Zaas AK, Schell WA, Betancourt-Quiroz M, Gunatilaka AA, Perfect JR, and Cowen LE (2010) PKC signaling regulates drug resistance of the fungal pathogen Candida albicans via circuitry comprised of Mkc1, calcineurin, and Hsp90. PLoS pathogens 6: e1001069. [PubMed: 20865172]

Lamoth F, Juvvadi PR, Fortwendel JR, and Steinbach WJ (2012) Heat shock protein 90 is required for conidiation and cell wall integrity in Aspergillus fumigatus. Eukaryotic cell 11: 1324–1332. [PubMed: 22822234]

Lamoth F, Juvvadi PR, Gehrke C, Asfaw YG, and Steinbach WJ (2014a) Transcriptional activation of heat shock protein 90 mediated via a proximal promoter region as trigger of caspofungin resistance in Aspergillus fumigatus. The Journal of infectious diseases 209: 473–481. [PubMed: 24096332]

Lamoth F, Juvvadi PR, Soderblom EJ, Moseley MA, Asfaw YG, and Steinbach WJ (2014b) Identification of a key lysine residue in heat shock protein 90 required for azole and echinocandin resistance in Aspergillus fumigatus. Antimicrobial agents and chemotherapy 58: 1889–1896. [PubMed: 24395240]

Lamoth F, Juvvadi PR, Soderblom EJ, Moseley MA, and Steinbach WJ (2015) Hsp70 and the Cochaperone StiA (Hop) Orchestrate Hsp90-Mediated Caspofungin Tolerance in Aspergillus fumigatus. Antimicrobial agents and chemotherapy 59: 4727–4733. [PubMed: 26014950]

Lamoth F, Juvvadi PR, and Steinbach WJ (2016) Heat shock protein 90 (Hsp90): A novel antifungal target against Aspergillus fumigatus. Crit Rev Microbiol 42: 310–321. [PubMed: 25243616]

Latge JP, and Chamilos G (2019) Aspergillus fumigatus and Aspergillosis in 2019. Clin Microbiol Rev 33.

Leach MD, Budge S, Walker L, Munro C, Cowen LE, and Brown AJ (2012a) Hsp90 orchestrates transcriptional regulation by Hsf1 and cell wall remodelling by MAPK signalling during thermal adaptation in a pathogenic yeast. PLoS pathogens 8: e1003069. [PubMed: 23300438]

Leach MD, Klipp E, Cowen LE, and Brown AJ (2012b) Fungal Hsp90: a biological transistor that tunes cellular outputs to thermal inputs. Nat Rev Microbiol 10: 693–704. [PubMed: 22976491]

Leach MD, Tyc KM, Brown AJ, and Klipp E (2012c) Modelling the regulation of thermal adaptation in Candida albicans, a major fungal pathogen of humans. PLoS One 7: e32467. [PubMed: 22448221]

Li J, Soroka J, and Buchner J (2012) The Hsp90 chaperone machinery: conformational dynamics and regulation by co-chaperones. Biochimica et biophysica acta 1823: 624–635. [PubMed: 21951723]

Livak KJ, and Schmittgen TD (2001) Analysis of relative gene expression data using real-time quantitative PCR and the 2(-Delta Delta C(T)) Method. Methods 25: 402–408. [PubMed: 11846609]

Luo Q, Boczek EE, Wang Q, Buchner J, and Kaila VR (2017) Hsp90 dependence of a kinase is determined by its conformational landscape. Sci Rep 7: 43996. [PubMed: 28290541]

Malavazi I, and Goldman GH (2012) Gene disruption in Aspergillus fumigatus using a PCR-based strategy and in vivo recombination in yeast. Methods in molecular biology 845: 99–118. [PubMed: 22328370]

Manfiolli AO, dos Reis TF, de Assis LJ, de Castro PA, Silva LP, Hori JI, Walker LA, Munro CA, Rajendran R, Ramage G, and Goldman GH (2018) Mitogen activated protein kinases (MAPK) and protein phosphatases are involved in Aspergillus fumigatus adhesion and biofilm formation. The Cell Surface 1: 43–56. [PubMed: 32743127]

McClellan AJ, Xia Y, Deutschbauer AM, Davis RW, Gerstein M, and Frydman J (2007) Diverse cellular functions of the Hsp90 molecular chaperone uncovered using systems approaches. Cell 131: 121–135. [PubMed: 17923092]

Minari K, de Azevedo EC, Kiraly VTR, Batista FAH, de Moraes FR, de Melo FA, Nascimento AS, Gava LM, Ramos CHI, and Borges JC (2019) Thermodynamic analysis of interactions of the Hsp90 with adenosine nucleotides: A comparative perspective. Int J Biol Macromol 130: 125–138. [PubMed: 30797004]

Moss BJ, Kim Y, Nandakumar MP, and Marten MR (2008) Quantifying metabolic activity of filamentous fungi using a colorimetric XTT assay. Biotechnol Prog 24: 780–783. [PubMed: 18386938]

Newton AC (2018) Protein kinase C: perfectly balanced. Crit Rev Biochem Mol Biol 53: 208–230. [PubMed: 29513138]

Nicholls S, Leach MD, Priest CL, and Brown AJ (2009) Role of the heat shock transcription factor, Hsf1, in a major fungal pathogen that is obligately associated with warm-blooded animals. Molecular microbiology 74: 844–861. [PubMed: 19818013]

Nomura W, Ito Y, and Inoue Y (2017) Role of phosphatidylserine in the activation of Rho1-related Pkc1 signaling in Saccharomyces cerevisiae. Cell Signal 31: 146–153. [PubMed: 28065784]

Nonaka H, Tanaka K, Hirano H, Fujiwara T, Kohno H, Umikawa M, Mino A, and Takai Y (1995) A downstream target of RHO1 small GTP-binding protein is PKC1, a homolog of protein kinase C, which leads to activation of the MAP kinase cascade in Saccharomyces cerevisiae. EMBO J 14: 5931–5938. [PubMed: 8846785]

O'Meara TR, O'Meara MJ, Polvi EJ, Pourhaghighi MR, Liston SD, Lin ZY, Veri AO, Emili A, Gingras AC, and Cowen LE (2019) Global proteomic analyses define an environmentally contingent Hsp90 interactome and reveal chaperone-dependent regulation of stress granule proteins and the R2TP complex in a fungal pathogen. PLoS Biol 17: e3000358. [PubMed: 31283755]

Perfect JR, Cox GM, Lee JY, Kauffman CA, de Repentigny L, Chapman SW, Morrison VA, Pappas P, Hiemenz JW, Stevens DA, and Mycoses Study G (2001) The impact of culture isolation of Aspergillus species: a hospital-based survey of aspergillosis. Clin Infect Dis 33: 1824–1833. [PubMed: 11692293]

Philipova R, and Whitaker M (2005) Active ERK1 is dimerized in vivo: bisphosphodimers generate peak kinase activity and monophosphodimers maintain basal ERK1 activity. J Cell Sci 118: 5767–5776. [PubMed: 16317051]

Rhodes JC (2006) Aspergillus fumigatus: growth and virulence. Med Mycol 44 Suppl 1: S77–81. [PubMed: 17050423]

Rhodes JC, and Askew DS, (2010) Aspergillus fumigatus In: Cellular and Molecular Biology of Filamentous Fungi. Borkovich KA & Ebbole DJ (eds). Washington: ASM Press, pp. 697–716.

Richie DL, Hartl L, Aimanianda V, Winters MS, Fuller KK, Miley MD, White S, McCarthy JW, Latge JP, Feldmesser M, Rhodes JC, and Askew DS (2009) A role for the unfolded protein response (UPR) in virulence and antifungal susceptibility in Aspergillus fumigatus. PLoS pathogens 5: e1000258. [PubMed: 19132084]

Rocha MC, de Godoy KF, Bannitz-Fernandes R, Fabri J, Barbosa MMF, de Castro PA, Almeida F, Goldman GH, da Cunha AF, Netto LES, de Oliveira MA, and Malavazi I (2018) Analyses of the three 1-Cys Peroxiredoxins from Aspergillus fumigatus reveal that cytosolic Prx1 is central to H2O2 metabolism and virulence. Sci Rep 8: 12314. [PubMed: 30120327]

Rocha MC, Fabri J, Simoes IT, Silva-Rocha R, Hagiwara D, da Cunha AF, Goldman GH, Canovas D, and Malavazi I (2020) The Cell Wall Integrity Pathway Contributes to the Early Stages of Aspergillus fumigatus Asexual Development. Applied and environmental microbiology 86.

Rocha MC, Fabri JH, Franco de Godoy K, Alves de Castro P, Hori JI, Ferreira da Cunha A, Arentshorst M, Ram AF, van den Hondel CA, Goldman GH, and Malavazi I (2016) Aspergillus fumigatus MADS-Box Transcription Factor rlmA Is Required for Regulation of the Cell Wall Integrity and Virulence. G3 (Bethesda) 6: 2983–3002. [PubMed: 27473315]

Rocha MC, Godoy KF, de Castro PA, Hori JI, Bom VL, Brown NA, Cunha AF, Goldman GH, and Malavazi I (2015) The Aspergillus fumigatus pkcA G579R Mutant Is Defective in the Activation of the Cell Wall Integrity Pathway but Is Dispensable for Virulence in a Neutropenic Mouse Infection Model. PLoS One 10: e0135195. [PubMed: 26295576]

Rueden CT, Schindelin J, Hiner MC, DeZonia BE, Walter AE, Arena ET, and Eliceiri KW (2017) ImageJ2: ImageJ for the next generation of scientific image data. BMC Bioinformatics 18: 529. [PubMed: 29187165]

Ryckbosch SM, Wender PA, and Pande VS (2017) Molecular dynamics simulations reveal ligand-controlled positioning of a peripheral protein complex in membranes. Nature Communications 8: 6.

Samantaray S, Neubauer M, Helmschrott C, and Wagener J (2013) Role of the guanine nucleotide exchange factor Rom2 in cell wall integrity maintenance of Aspergillus fumigatus. Eukaryotic cell 12: 288–298. [PubMed: 23264643]

Schindelin J, Arganda-Carreras I, Frise E, Kaynig V, Longair M, Pietzsch T, Preibisch S, Rueden C, Saalfeld S, Schmid B, Tinevez J-Y, White DJ, Hartenstein V, Eliceiri K, Tomancak P, and Cardona A (2012) Fiji: an open-source platform for biological-image analysis. Nature Methods 9: 676–682. [PubMed: 22743772]

Schmitz HP, and Heinisch JJ (2003) Evolution, biochemistry and genetics of protein kinase C in fungi. Current genetics 43: 245–254. [PubMed: 12736758]

Schmitz HP, Jockel J, Block C, and Heinisch JJ (2001) Domain shuffling as a tool for investigation of protein function: substitution of the cysteine-rich region of Raf kinase and PKC eta for that of yeast Pkc1p. Journal of molecular biology 311: 1–7. [PubMed: 11469853]

Schneider CA, Rasband WS, and Eliceiri KW (2012) NIH Image to ImageJ: 25 years of image analysis. Nat Methods 9: 671–675. [PubMed: 22930834]

Schopf FH, Biebl MM, and Buchner J (2017) The HSP90 chaperone machinery. Nat Rev Mol Cell Biol 18: 345–360. [PubMed: 28429788]

Seraphim TV, Silva KP, Dores-Silva PR, Barbosa LR, and Borges JC (2017) Insights on the structural dynamics of Leishmania braziliensis Hsp90 molecular chaperone by small angle X-ray scattering. Int J Biol Macromol 97: 503–512. [PubMed: 28104372]

Silva KP, Seraphim TV, and Borges JC (2013) Structural and functional studies of Leishmania braziliensis Hsp90. Biochimica et biophysica acta 1834: 351–361. [PubMed: 22910377]

Singh SD, Robbins N, Zaas AK, Schell WA, Perfect JR, and Cowen LE (2009) Hsp90 governs echinocandin resistance in the pathogenic yeast Candida albicans via calcineurin. PLoS pathogens 5: e1000532. [PubMed: 19649312]

Sueiro-Olivares M, Fernandez-Molina JV, Abad-Diaz-de-Cerio A, Gorospe E, Pascual E, Guruceaga X, Ramirez-Garcia A, Garaizar J, Hernando FL, Margareto J, and Rementeria A (2015) Aspergillus fumigatus transcriptome response to a higher temperature during the earliest steps of germination monitored using a new customized expression microarray. Microbiology 161: 490–502. [PubMed: 25536999]

Sugui JA, Kwon-Chung KJ, Juvvadi PR, Latge JP, and Steinbach WJ (2014) Aspergillus fumigatus and related species. Cold Spring Harb Perspect Med 5: a019786. [PubMed: 25377144]

Taipale M, Jarosz DF, and Lindquist S (2010) HSP90 at the hub of protein homeostasis: emerging mechanistic insights. Nat Rev Mol Cell Biol 11: 515–528. [PubMed: 20531426]

Taipale M, Krykbaeva I, Koeva M, Kayatekin C, Westover KD, Karras GI, and Lindquist S (2012) Quantitative analysis of HSP90-client interactions reveals principles of substrate recognition. Cell 150: 987–1001. [PubMed: 22939624]

Teepe AG, Loprete DM, He Z, Hoggard TA, and Hill TW (2007) The protein kinase C orthologue PkcA plays a role in cell wall integrity and polarized growth in Aspergillus nidulans. Fungal Genet Biol 44: 554–562. [PubMed: 17118679]

Valiante V, Jain R, Heinekamp T, and Brakhage AA (2009) The MpkA MAP kinase module regulates cell wall integrity signaling and pyomelanin formation in Aspergillus fumigatus. Fungal Genet Biol 46: 909–918. [PubMed: 19715768]

Valiante V, Macheleidt J, Foge M, and Brakhage AA (2015) The Aspergillus fumigatus cell wall integrity signaling pathway: drug target, compensatory pathways, and virulence. Front Microbiol 6: 325. [PubMed: 25932027]

van de Veerdonk FL, Gresnigt MS, Romani L, Netea MG, and Latge JP (2017) Aspergillus fumigatus morphology and dynamic host interactions. Nat Rev Microbiol 15: 661–674. [PubMed: 28919635]

Wang B, Qin X, Wu J, Deng H, Li Y, Yang H, Chen Z, Liu G, and Ren D (2016) Analysis of crystal structure of Arabidopsis MPK6 and generation of its mutants with higher activity. Sci Rep 6: 25646. [PubMed: 27160427]

Weber DJ, Peppercorn A, Miller MB, Sickbert-Benett E, and Rutala WA (2009) Preventing healthcare-associated Aspergillus infections: review of recent CDC/HICPAC recommendations. Med Mycol 47 Suppl 1: S199–209. [PubMed: 19274596]

Wu Y, Li Q, and Chen XZ (2007) Detecting protein-protein interactions by Far western blotting. Nat Protoc 2: 3278–3284. [PubMed: 18079728]

Zhao R, Davey M, Hsu YC, Kaplanek P, Tong A, Parsons AB, Krogan N, Cagney G, Mai D, Greenblatt J, Boone C, Emili A, and Houry WA (2005) Navigating the chaperone network: an integrative map of physical and genetic interactions mediated by the hsp90 chaperone. Cell 120: 715–727. [PubMed: 15766533]

Zhou H, Hu H, Zhang L, Li R, Ouyang H, Ming J, and Jin C (2007) O-Mannosyltransferase 1 in Aspergillus fumigatus (AfPmt1p) is crucial for cell wall integrity and conidium morphology, especially at an elevated temperature. Eukaryotic cell 6: 2260–2268. [PubMed: 17905922]

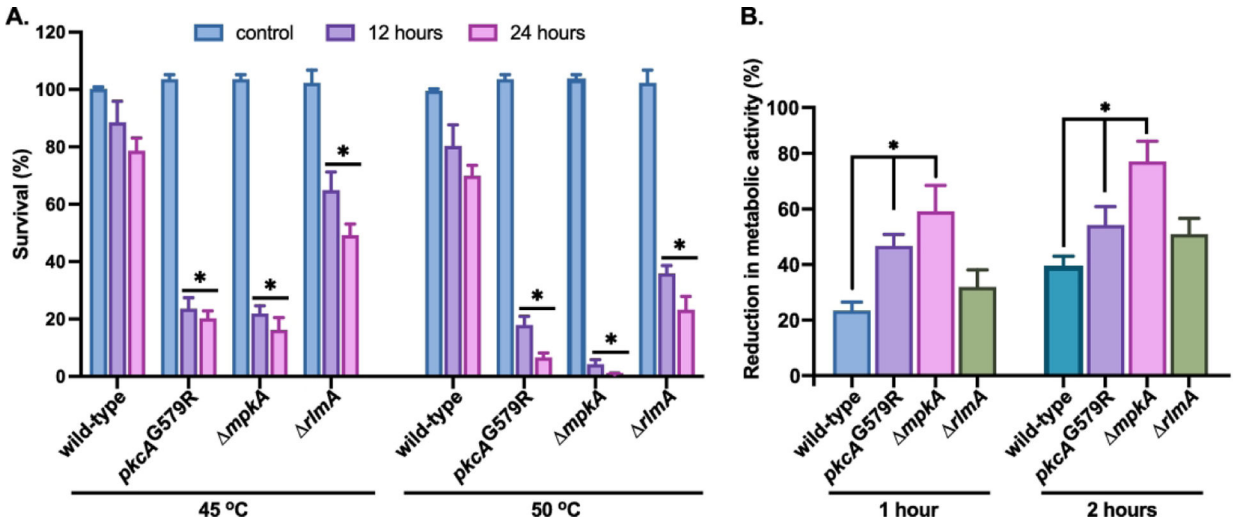

Figure 1. CWIP genes contribute to thermotolerant growth.

(A) 1×10^2 conidia of each strain were exposed to temperatures of 45 °C and 50 °C for 12 and 24 h in Petri dishes containing solid MM. Subsequently, the plates were incubated at 37 °C for recovery for 24 h. The percentage of viable colonies was obtained in comparison to the non-HS control (30 °C). (B) The XTT assay was used to measure the metabolic activity of mature biofilm of CWIP mutants. The biofilms were obtained by growing each strain for 22 h in MM at 37 °C in 24-well plates. Biofilms were then incubated for 2 h at 30 °C. Subsequently, the plates were heat-shocked at 48 °C for the indicated times. The results were expressed as mean ± SD, n = 4. * $p \leq 0.01$ One-way ANOVA and Dunnett's posttest.

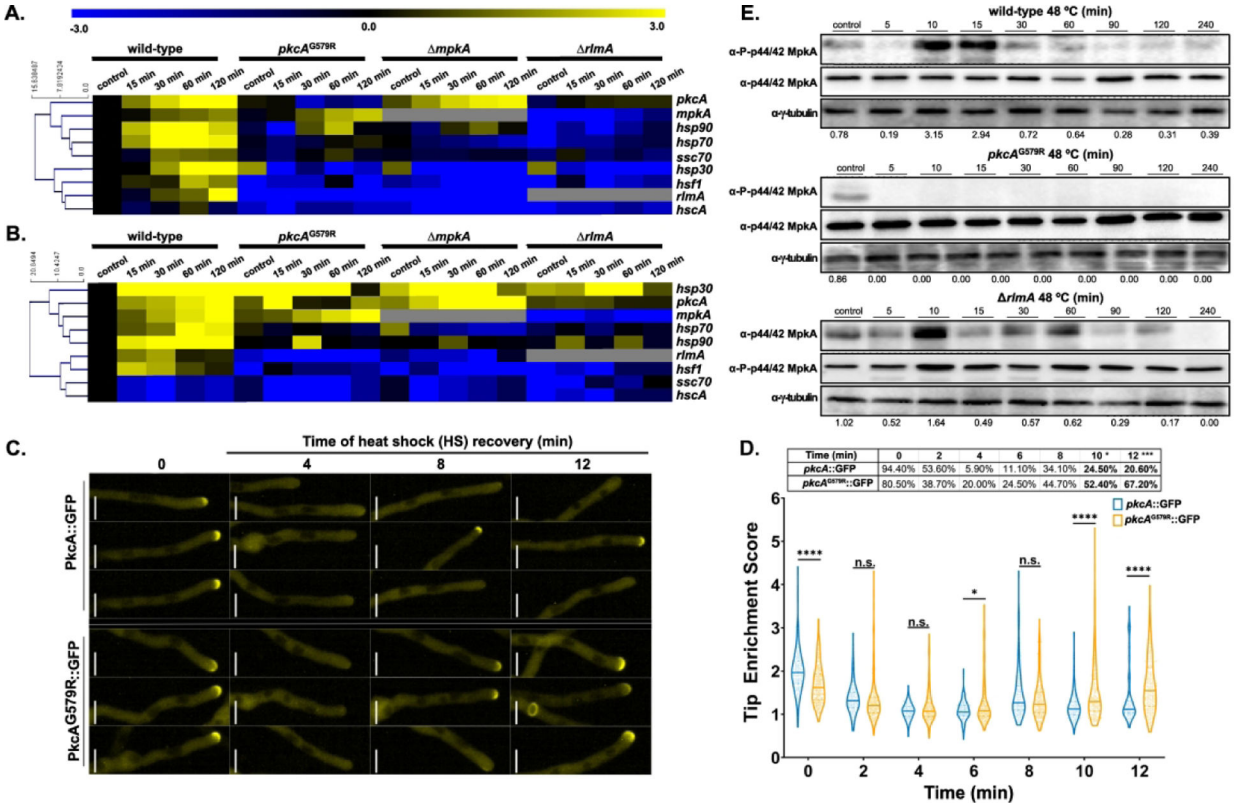

Time (min)	0	2	4	6	8	10 *	12 ***
pkcA::GFP	94.40%	53.60%	5.90%	11.10%	34.10%	**24.50%**	**20.60%**
pkcA^{G579R}::GFP	80.50%	38.70%	20.00%	24.50%	44.70%	**52.40%**	**67.20%**

Figure 2. The CWIP coordinates cell responses to thermal adaptation and PkcA-dependent MpkA phosphorylation is critical to protect cells from HS at 48 °C.

(A-B) The CWIP mutant strains present lower mRNA abundance of genes encoding the major heat shock proteins. Expression of *pkcA*, *mpkA*, *rlmA*, *hsp30*, *hsp90*, *hsfA*, *hsp70*, *ssc70,* and *hscA* was investigated by RT-qPCR in the strains subjected to heat shock during the indicated time points (h) at 37 °C (A) and 48 °C (B). Values represent the average $\log_2$-fold change relative to the control cDNA (30 °C) for a specific gene compared to the same time point of the wild-type strain (n=3 with 2 technical repetitions each; see Fig. S1 for statistics). The values were submitted to a hierarchical clustering algorithm (Euclidian distance) by using the WebMeV platform. (C) PkcA localizes at the hyphal tips, septum and sites of new growth under physiological conditions, reallocates to the cytosol after HS and eventually returns to the natural accumulation sites after HS recovery. The conidia of each strain were inoculated in MM and incubated at 37 °C for 10 h and room temperature for 1 h. Media was removed and replaced by fresh pre-warmed media at 48 °C to induce HS. Recovery of the fluorescence was followed by the time indicated in the panels. Experiments were independently repeated at least four times and representative germlings of a single experiment are shown. Fluorescence was artificially colored in yellow to enhance visualization. Scale bars = 5 μm. (D) Violin plot of the tip enrichment scores of *pkcA*::GFP and *pkcA*^{G579R}::GFP strains. The mutant protein has a lower degree of enrichment at hyphal tips under physiological conditions (0 min) while it regains baseline tip localization sooner in comparison to the wild-type isoform. The upper table indicate the percent of hyphal tips containing tip localized PkcA at the population level obtained from the average across biological replicates (n = 4 for *pkcA*::GFP and n = 6 for *pkcA*^{G579R}::GFP). Differences in

the return of tip localization between the two alleles is seen at 10- and 12-minutes post-HS. For both metrics, statistics were determined by two-way ANOVA with a Sidak's multiple comparison test. **** $p<0.0001$, * $p<0.05$, n.s. not significant. (E) The strains were cultured for 24 h in MM at 30 °C. Subsequently, the mycelium was transferred to fresh pre-heated MM and incubated at 48 °C for the indicated times. The phosphorylated and the total MpkA amount were detected using α-P-p44/42 and α-p44/42 MAPK antibodies, respectively. The α-γ-tubulin antibody was used as loading sample control. Values indicate the ratio of phosphorylated/non-phosphorylated MpkA. Representative images of three independent experiments.

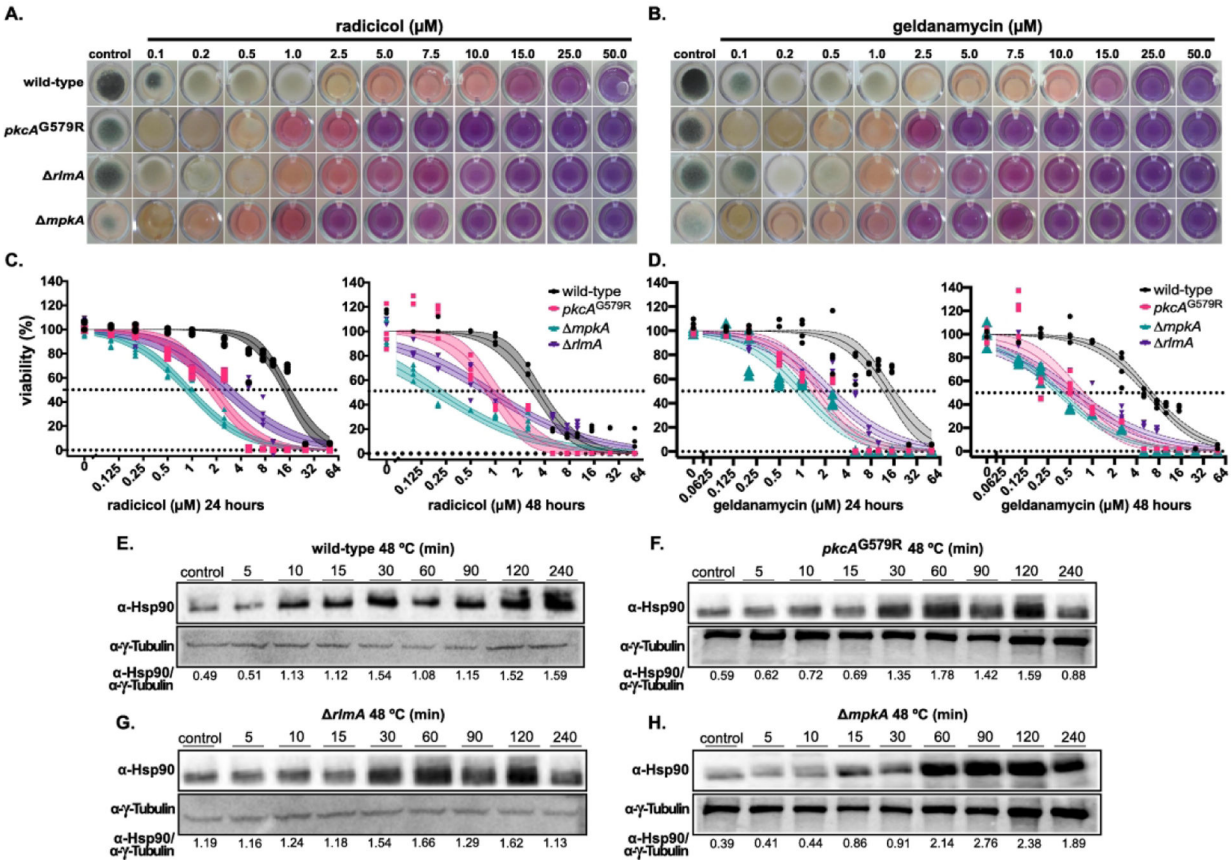

Figure 3. The CWIP mutants are sensitive to Hsp90 inhibition and present late expression of Hsp90 after HS.

(A-B) 1×10^3 conidia of the wild-type and CWIP mutants were inoculated in liquid MM supplemented with different concentrations of radicicol and geldanamycin for 48 h at 37 °C. (C-D) Viability after 24 h and 48 h of incubation (37 °C) was quantified by fluorescence of the reduced alamar blue indicator added to each well. Dashed lines indicate the calculated IC_{50} and shaded areas on each curve indicated the 95% confidence interval. (E-H) Hsp90 protein abundance during HS. The strains were grown for 24 h in MM at 30 °C and subsequently heat-shocked at 48 °C for the indicated timepoints. An α-Hsp90 polyclonal antibody was used to detect Hsp90 and γ-tubulin antibody was used as the loading control. Values indicate the ratio of Hsp90/ γ-tubulin signals. Results are representative images of three independent experiments.

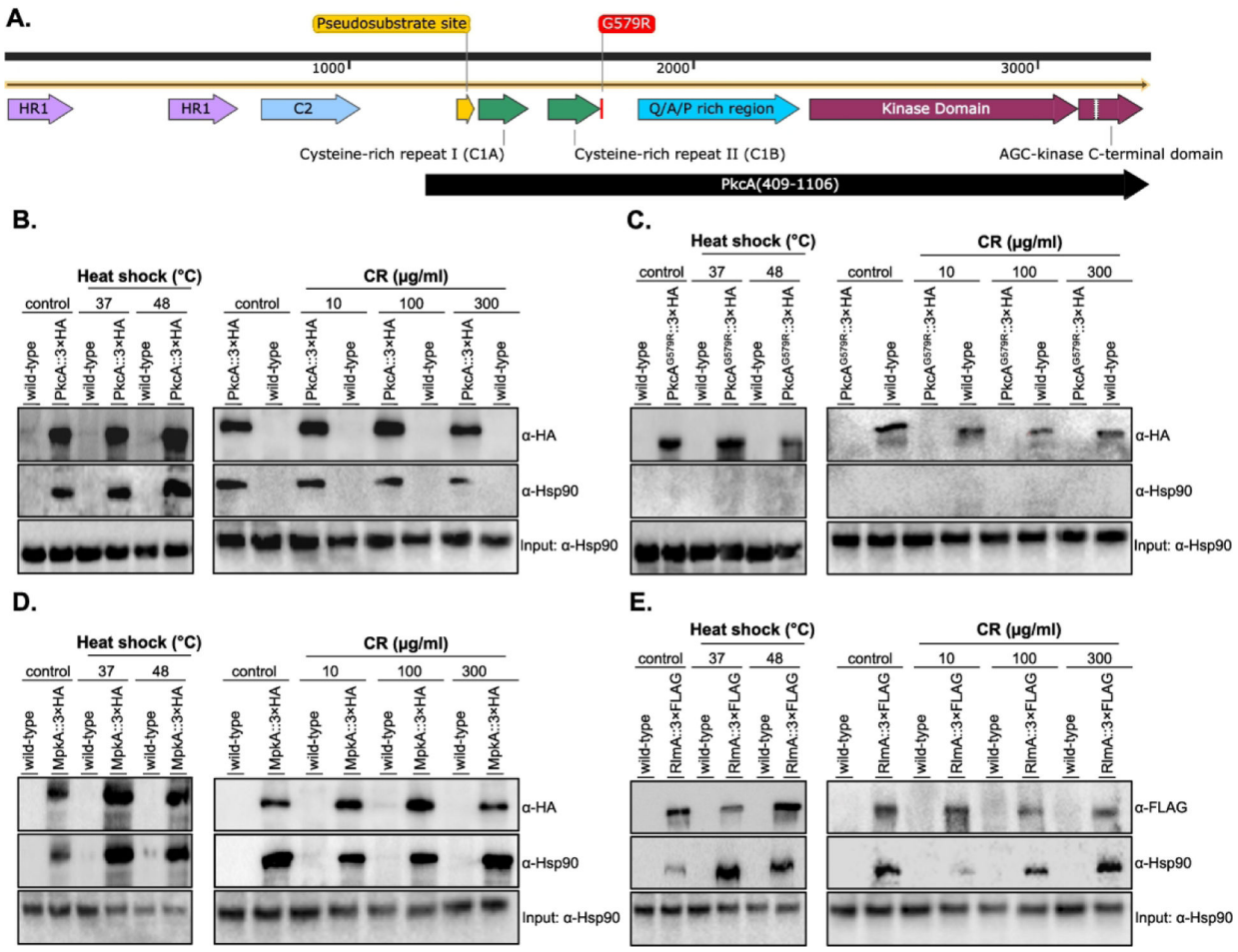

Figure 4. The CWIP proteins PkcA, MpkA and RlmA are constitutive Hsp90 clients in *A. fumigatus*.

(A) Domains and structural organization of PkcA sequence. The location of the Gly579, which is mutated to an Ala in the PkcA^{G579R} mutant, is highlighted in the red box. It is the first residue juxtaposed after the C1B domain in the primary sequence of the polypeptide. The black arrow indicates the C-terminal truncated version of the polypeptide, PkcA(409–1106), expressed in bacterial system (see text for details). PkcA(409–1106) contained the pseudosubstrate site (yellow), the C1 domain, which comprises the cysteine-rich repeats C1A and C1B (green), the fungal specific Q/A/P-rich region (blue) and the catalytic domain of the enzyme (magenta). The structure of PkcA was deduced from Prosite scan and from comparison to other fungi based on (Herrmann *et al.*, 2006, Teepe *et al.*, 2007, Heinisch & Rodicio, 2018). The white segment inside the C-terminal domain indicates the localization of the PxxP region, which is described as necessary for Hsp90 and Cdc37 in mammalian cells (Gould *et al.*, 2009). Identification of PxxP was based in comparison to human PkcA-α (NCBI accession number P17252.4, see text for details). Black and yellow lines indicate the cDNA and polypeptide sequences, respectively. The wild-type and *pkcA::*3×HA (B), *pkcA*^{G579R}*::*3×HA (C), *mpkA::*3×HA (D) and *rlmA::*3×FLAG (E) tagged strains were used in the Co-IP assays. Strains were grown at 30 °C (24 h) and subsequently upshifted to 37 °C or 48 °C for 15 min to induce HS (left panels). To induce CW stress, strains were grown at

37 °C (22 h) and subsequently exposed to 10, 100 or 300 μg/mL of congo red (CR) for 30 min (right panels). Dynabeads protein A bound to the α-HA antibody or α-Flag M2 Affinity gel were used to immunoprecipitated MpkA and PkcA or RlmA, respectively. Co-immunoprecipitated Hsp90 was investigated by Western blot analysis using α-Hsp90 antibody. Hsp90 was also used as the input control for all the samples. Predicted fusion protein sizes on the blot: MpkA::3×HA: 51.4 kDa; PkcA and PkcA^{G579R}: 127.1 kDa; RlmA::3×FLAG: 70.3; Hsp90: 80.6 kDa.

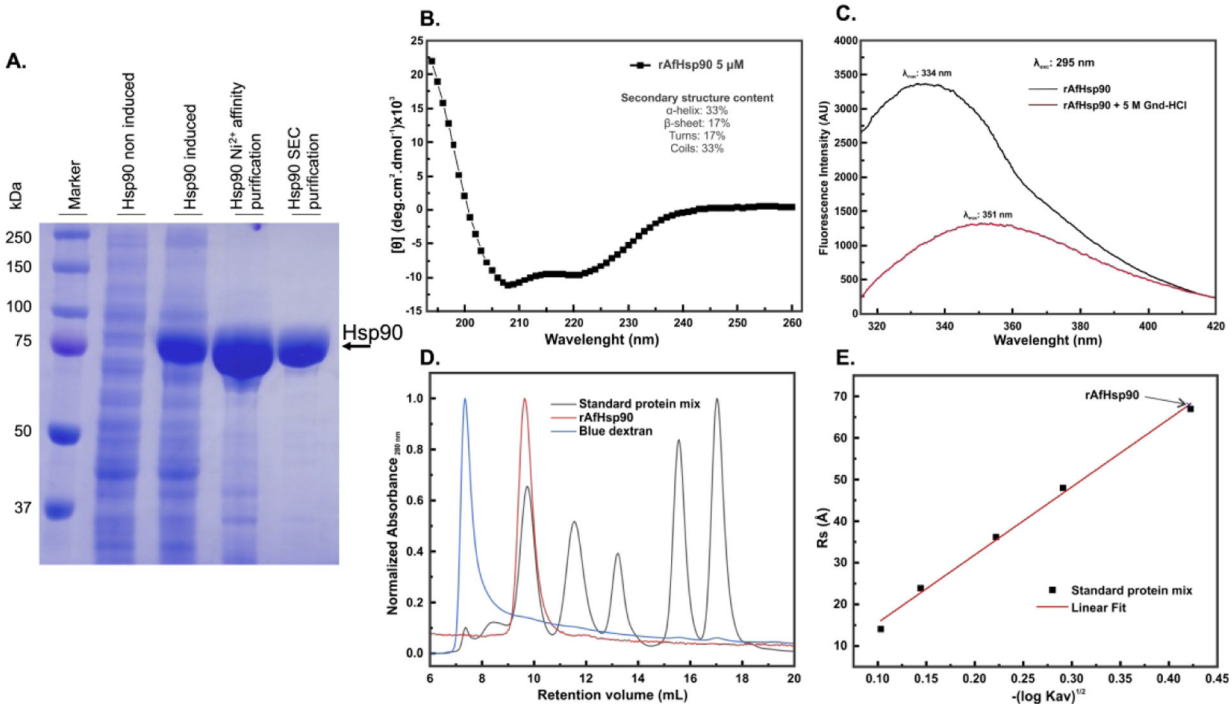

Figure 5. Protein purification and spectroscopic characterization of Hsp90.

(A) 10% SDS-PAGE showing Hsp90 expression (arrow) in *E. coli* before and after IPTG induction (lanes 2 and 3, respectively), proteins eluted from Ni^{+2}-affinity chromatography (lane 4) and after size exclusion chromatography (SEC; lane 5). The marker of MW is shown in lane 1. (B) CD spectrum of rAfHsp90 acquired in the buffer 40 mM HEPES (pH 7.5), 100 mM KCl, and normalized for mean molar residual ellipticity. (C) Intrinsic fluorescence spectroscopy experiments using the rAfHsp90 protein, in the presence and absence of guanidine hydrochloride (Gnd-HCl). The fluorescence emission spectra reflect the local tertiary environment of the Trp residues. (D) aSEC elution profile for rAfHsp90 and the standard protein mixture. rAfHsp90 eluted with a retention volume similar to apoferritin. Molecular size of standard proteins: apoferritin (480 kDa), γ-globulin (160 kDa), bovine serum albumin (BSA 67 kDa), carbonic anhydrase (30 kDa) and cytochrome C (12.3 kDa). The blue dextran elution profile identifies the void volume. (E) The retention volumes observed for the standard proteins were transformed into the Kav and plotted against the Rs of the standard proteins to determine the Rs for rAfHsp90.

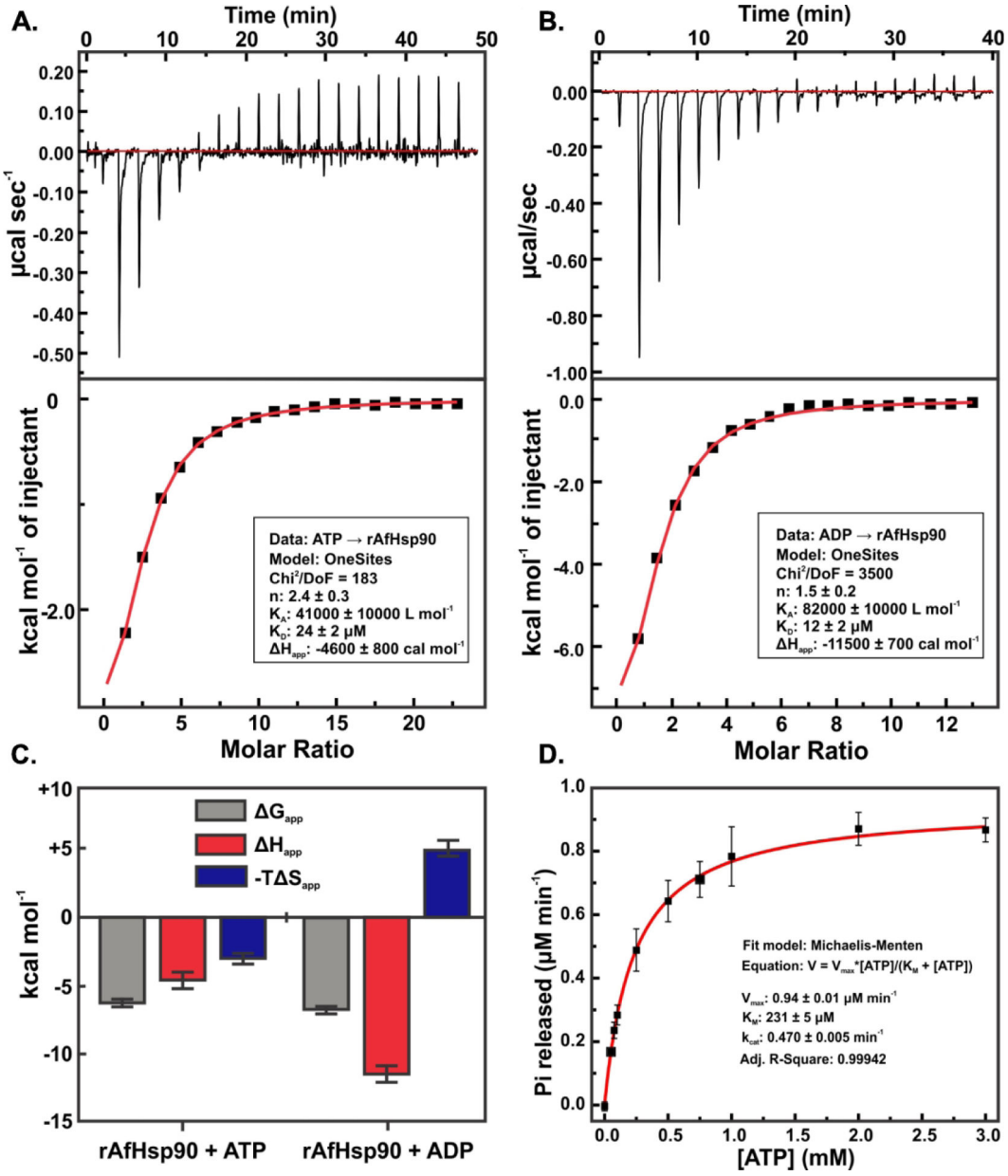

Figure 6. rAfHsp90 binds to the natural ligands ATP and ADP and is a functional ATPase.

The binding of Hsp90 with ATP and ADP was investigated by ITC at 25 °C. ATP (A) or ADP (B) were titrated into the buffer containing the rAfHsp90 generating characteristic thermograms of exothermic reactions. The lower panels indicate the best fitting routine, which yielded values for n, K_A and ΔH_{app} (C) The calorimetric values for apparent ΔH, ΔG and TΔH resulting from the rAfHsp90 binding to ATP and ADP. The ΔH_{app} was more than twice higher for ADP binding in comparison to the ATP. (D) Enzyme kinetics of AfHsp90 ATPase activity. AfHsp90 (2 µM) was incubated with ATP (0 – 3 mM) during 90 min at 37 °C and the Pi released from ATP hydrolysis was quantified. The data were treated with a Michaelis-Menten fitting for the achievement of kinetic parameters (graph inset).

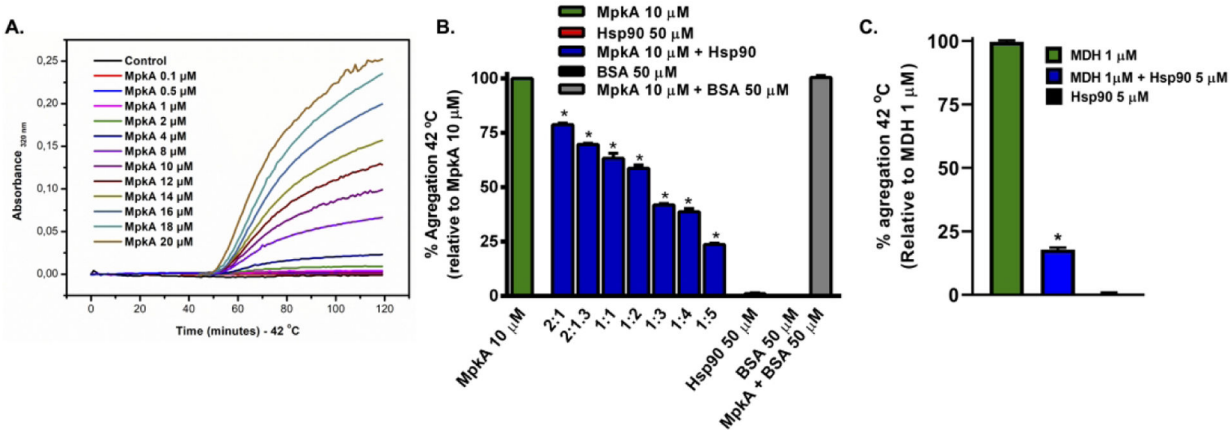

Figure 7. rAfHsp90 chaperons rAfMpkA *in vitro*.

The Hsp90 chaperone activity was assessed by monitoring the ability of rAfHsp90 to prevent aggregation of the client protein by light scattering at 320 nm for 4 h at 42 °C (A) Thermal stability studies of rAfMpkA indicates it aggregates after 120 min of incubation at 42 °C (40 mM HEPES (pH 7.5) buffer containing 100 mM KCl) in a concentration-dependent manner. (B) Inhibition of MpkA aggregation (%) calculated in the presence of 10 µM of rAfMpkA and increasing concentrations of rAfHsp90, *i.e*. 5 µM (2:1), 7.5 µM (2: 1.3), 10 µM (1:1), 20 µM (1:2), 30 µM (1:3), 40 µM (1:4) and 50 µM (1:5). Aggregation values were calculated considering the maximum aggregation of MpkA as 100%. (D) The human malate dehydrogenase (MDH, 1 µM), a known Hsp90 client, was used as a positive control of rAfHsp90 chaperone activity.

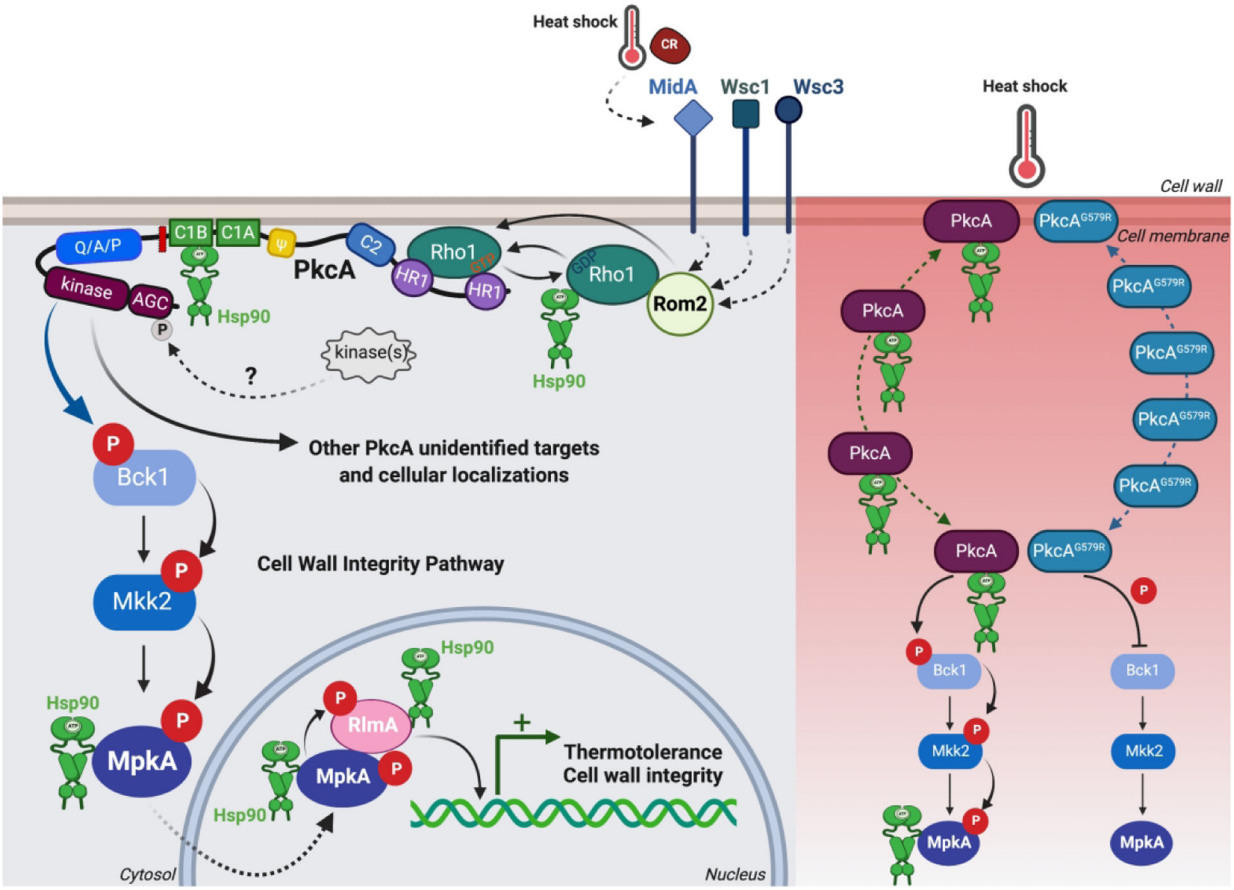

Figure 8. The Hsp90 association with the CWIP components is essential to *A. fumigatus* thermotolerance.

PkcA is shown in its activated form, according to the *S. cerevisiae* model. Activation occurs after the dissociation of the interaction between C1, C2 and pseudosubstrate site (ψ), possible after the priming phosphorylation of the protein at the C-terminal kinase (AGC kinase signature) domain (see text for details), by unidentified kinases in *A. fumigatus*. The domain organization of the protein and color scheme is shown as in Fig. 4A. The HS and congo red (CR) response is thought to emerge mainly from the MidA mechanosensor located at the cell membrane and funneled into Rom2, a guanine nucleotide exchange factor and the small Rho GTPAse Rho1, leading to the activation of PkcA. In the likely absence of DAG stimulation of fungal PkcA via C1 domain, Rho1 can be the linking component that tethers C1A and C1B PkcA domains to the cell membrane, thus suggesting the importance of C1B domain, where the G579R mutation is located (red line). This polypeptide region is important for the interaction of Hsp90 with PkcA since this interaction is abolished in the PkcA^{G579R} isoform (right). *A. fumigatus* Rho1 is also an Hsp90 client (data not shown in this study). For all recorded physical interactions, Hsp90 chaperone is shown as a homodimer (green) in its closed state, *i.e.,* bound to ATP since we recorded here all the structural and thermodynamic signatures of this protein and ATPase activity. PkcA activates unknown downstream targets in *A. fumigatus* and the MAP kinase cascade (green arrow), which ends in the quick activation of MpkA upon HS. MpkA is a constitutive Hsp90 client. The phosphorylation of MpkA is highly dependent on a fully functional PkcA (left). MpkA

migrates to the nucleus where it phosphorylates and activates the TF RlmA. RlmA is also an Hsp90 partner and the MpkA/Hsp90/RlmA complex reside in the nucleus under physiological or HS condition. Transcriptional targets of RlmA involved in the CW integrity and HS response are activated. HS (right) stimulates the migration (disappearance) of wild-type and mutated PkcA from the cytosol's hyphal tips. The return (recruitment) of $PkcA^{G579R}$ isoform is faster in comparison to the PkcA isoform. Although this model does not explain if PkcA located at the hyphal tip or other cell compartment under basal conditions is enzymatically active, the faster recruitment of $PkcA^{G579R}$ to the original sites may suggest an inefficient function of the mutated isoform due to the overall alterations in the polypeptide structure that potentially impacts the C1 domain. This diagram is based on data from this article and the following references (Dichtl *et al.*, 2012, Heinisch & Rodicio, 2018, Rocha *et al.*, 2020, Rocha *et al.*, 2016, Rocha *et al.*, 2015, Samantaray *et al.*, 2013, Schmitz & Heinisch, 2003, Valiante *et al.*, 2015). Created with BioRender.com.